

\\

**Grant Agreement number:** 101147454

**Project acronym:** DEMOQUAS

**Project title:** DEsigning, Manufacturing and Operating Quantification of Uncertainties to increase Aviation Safety

**Type of action:** HORIZON Research and Innovation Actions



## WP3 “Uncertainty quantification methods in design and development”

WP leader “ICL”

**T3.1** “UQ methods: gap analysis and development for life cycle phases”

**T3.2** “Uncertainty characterization for critical building blocks”

# Uncertainty quantification methods review & preliminary characterisation in H2-powered propulsion components [D3.1]

Delivery type:	Report
Lead beneficiary:	ICL
Lead authors:	ICL (Mehdi Anhichem, Francesco Montomoli, Vito Tagarielli)
Contributions:	AUTH (Michail Psaropoulos, George Arvithis, Konstantinos Bolas, Vasilis Gkoutzamanis, Anestis Kalfas), SAFRAN (Panagiotis Giannakakis, Manuel De Jesus Gurrola Arrieta), LSC (Paschalis Oikonomou, Panagiotis Tsirikoglou), ADV (George Maistros)
Contractual delivery date:	30 <sup>th</sup> of June 2025
Delivery date:	30 <sup>th</sup> of June 2025
Dissemination level:	PU – Public

### Information Table

Project Title	DEsigning, Manufacturing and Operating Quantification of Uncertainties to increase Aviation Safety
Project Acronym	DEMOQUAS
GA n.	101147454
Project Coordinator	Aristotelio Panepistimio Thessalonikis (AUTH)
Project Duration	36 months
Deliverable n.	D3.1
Deliverable title	Uncertainty quantification methods review & preliminary characterisation in H2-powered propulsion components
Deliverable description	R - Document, report Gap analysis with emphasis on open-libraries and detailing of methods in life cycle phases
Dissemination level	PU - Public
Work Package	WP3 – Coordination, Administration & EU Synergies
Task(s)	3.1/3.2
Lead Beneficiary	ICL
Contributing beneficiary/ies	All partners
Due date of deliverable (month)	14
Submission date	30 <sup>th</sup> of June 2025

### History of Changes

Version	Date	Author/Contributor	Changes
1.0	02/05/2025	ICL	Shared structure
2.0	30/05/2025	ICL	First draft completed and partners exchanging feedback
3.0	28/06/2025	ICL	Shared final document for final internal checks – Coordinator’s final check
4.0	30/06/2025	ICL	Uploaded to EU portal

### Disclaimer

The sole responsibility for the content of this publication lies with the authors. It does not necessarily reflect the opinion of the European Commission. The European Commission is not responsible for any use that may be made of the information contained therein.

### **Abbreviations and acronyms**

Abbreviation	Definition
Dx.x	Deliverable number x.x
UQ	Uncertainty Quantification
RUL	Remaining Useful Life
Tx.x	Task number x.x
WP(s)	Work Package(s)
Partner Acronym	Definition
ADV	Advise-Deta
AUTH	Aristotle University of Thessaloniki
BTC	B&T Composites
EGA	Egnatia Aviation
ICL	Imperial College London
ICO	ICOMAT
LSC	Limmat Scientific AG
MOD/MOD-G	Modelon/Modelon Deutschland
RRPLC	Rolls-Royce PLC
SAFRAN	SAFRAN
STAM	STAM SRL
TUD	TU Delft

# Table of contents

- Executive summary ..... 7
- 1. Introduction..... 8
  - 1.1. Purpose of the deliverable ..... 8
  - 1.2. Structure of the document ..... 9
- 2. Engineering design under uncertainty ..... 10
  - 2.1. Uncertainty quantification and propagation ..... 10
  - 2.2. Applications in industry ..... 11
  - 2.3. Challenges in applying uncertainty quantification ..... 12
- 3. Uncertainty quantification methods ..... 14
  - 3.1. Pseudo-random sampling methods..... 14
    - Monte Carlo method ..... 14
    - Latin Hypercube ..... 15
  - 3.2. Surrogate-based methods ..... 16
    - Gaussian processes..... 17
    - Polynomial chaos expansions..... 19
    - Neural networks ..... 20
  - 3.3. Multifidelity methods..... 22
  - 3.4. Sensitivity analysis ..... 24
    - Challenges ..... 24
    - Global sensitivity analysis..... 25
  - 3.5. Reliability methods ..... 28
  - 3.6. Application and software considerations ..... 29
- 4. Preliminary characterisation in H<sub>2</sub>-powered propulsion components ..... 31
  - 4.1. Design and development ..... 31
    - 4.1.1. Uncertainties in aircraft engine design..... 31
    - Effect of manufacturing tolerances ..... 32

Uncertainties during engine design phase.....	33
Uncertainties during aircraft design and due to potential engine growth.....	34
Uncertainties treatment in aircraft engine performance - Literature.....	34
DEMOQUAS proposed implementation .....	37
4.1.2. Uncertainties in thermal management systems .....	40
Description of Thermal Management System architecture .....	40
Uncertainty treatment in heat exchanger design: Effect of manufacturing tolerances .....	40
Uncertainty treatment in heat exchangers: Uncertainties of non-dimensional numbers.....	43
Uncertainty treatment in heat exchangers: Thermophysical properties .....	44
The problem of heat exchanger over-design .....	46
Effect of thermal management system cryogenic pumps .....	47
Preliminary identification of thermal management system key impactful parameters .....	48
4.2. Manufacturing and measuring.....	50
4.3. Operational aspects.....	51
Preliminary characterization of uncertainties concerning degradation and remaining useful life .....	51
Annex.....	56
Calculation of compact offset strip plate-fin heat exchanger dimensions .....	56

## List of Figures

<b>Figure 1.</b> Representation of uncertainty propagation using Monte Carlo sampling, where the uncertain inputs are drawn from Gaussian, triangular, and uniform distributions. ....	11
<b>Figure 2.</b> Monte Carlo and Latin Hypercube samples of $X \sim U(0,12)$ . ....	16
<b>Figure 3.</b> Gaussian process example with representative mean and confidence interval. ....	18
<b>Figure 4.</b> Example of multilayer perceptron with three hidden layers. ....	21
<b>Figure 5.</b> Thermal Management System architecture considered for the investigation. ....	40
<b>Figure 6.</b> Typical offset strip plate-fin heat exchanger geometry considered for the Thermal Management System. ....	41
<b>Figure 7.</b> Maximum uncertainty range for the hydraulic diameter (a), the fin-to-total area ratio (b) and the total heat transfer area-to-volume ratio (c) estimated for the selected dataset of heat exchangers, based on the respective design tolerances. ....	42
<b>Figure 8.</b> Gaussian distributions for the key operational input parameters of the cryogenic pumps (a, b, c) and the resulting effect on the overall pump power requirements (d). Despite exhibiting a non-negligible relative uncertainty, the overall power is still insignificant compared to the engine thrust power. ....	47
<b>Figure 9.</b> Resulting global total-order sensitivity indices of all the investigated parameters related to the TMS model. ....	48
<b>Figure 10.</b> RUL process for aeroengines. ....	52
<b>Figure 11.</b> Illustration of three engine units presenting average, accelerated, and extended deterioration. ....	53

## List of Tables

<b>Table 1.</b> Characterization of engine design uncertainties related to manufacturing deviations, according to existing literature ....	33
<b>Table 2.</b> Characterization of engine design uncertainties due to engine-to-engine scatter, according to existing literature. ....	34
<b>Table 3.</b> Evaluation metrics in the rotation speed estimation. ....	36
<b>Table 4.</b> Summary of key outcomes of selected studies in existing literature, regarding the uncertainty quantification of gas turbines and aircraft engines. ....	37
<b>Table 5.</b> Turbine Entry Temperature margin stack-up due to various sources of uncertainty according to literature. ....	38
<b>Table 6.</b> Summary of proposed preliminary characterization of engine performance uncertainties. ....	39
<b>Table 7.</b> Selected tolerances for the heat exchanger dimensions in the design phase. ....	43

**Table 8.** Summary of key uncertainties in the non-dimensional numbers for various compact heat exchanger geometries reported by Kays and London..... 43

**Table 9.** Summary of thermophysical properties uncertainties reported for various mediums used in Thermal Management Systems. .... 46

**Table 10.** First-order and Total-order global sensitivity indices for the key influential parameters of the Thermal Management System. .... 49

**Table 11.** Uncertainties due to composite’s quality monitoring. .... 50

**Table 12.** Uncertainties due to measurements. .... 51

## Executive summary

This document constitutes the first deliverable of Work Package 3 (WP3) of the DEMOQUAS project and serves as a report on the review and exploratory work conducted during the project's first year. Its primary objective is to establish a shared understanding of uncertainty quantification (UQ) methods and challenges within the context of hydrogen-powered aviation systems. The document begins with an overview of the role and importance of UQ in industrial applications, particularly in complex engineering systems. It is then structured around two main axes. The first part provides a comprehensive review of state-of-the-art UQ methods—including sampling-based techniques, surrogate modelling, and multi-fidelity approaches—that are being leveraged across various tasks of the project. The second part presents a preliminary characterization of the uncertainties associated with the key components of hydrogen-powered propulsion systems. This includes a discussion of system fidelity, lifecycle stages, and sources of epistemic and aleatoric uncertainties. Notably, this second part has been developed collaboratively with input from all project partners, reflecting a multidisciplinary effort to align modelling, measurement, and design perspectives. This deliverable lays the foundation for the more detailed UQ developments and implementations that will follow in subsequent stages of WP3.

# 1. Introduction

## 1.1. Purpose of the deliverable

This deliverable represents an initial step in advancing WP3 of the DEMOQUAS project by presenting a comprehensive review of uncertainty quantification methods, some of which will be applied throughout the project. It also offers a preliminary update on the characterisation of uncertainties across various systems, considering their level of fidelity and corresponding stages in the system life cycle. The purpose of this document is to support the tasks 3.1 and 3.2 of WP3 by providing a foundational review and preliminary analysis of uncertainty quantification methods and their relevance to hydrogen-powered propulsion systems. It aims to establish a common understanding across project partners of the methodological tools and conceptual frameworks needed to characterize, propagate, and reduce uncertainties in the design and development of complex aerospace systems. Specifically, this document serves to:

- **Review state-of-the-art UQ methods** relevant to the challenges faced in aerospace engineering, with an emphasis on techniques that are applicable to high-dimensional, nonlinear, and multi-fidelity systems.
- **Identify and assess UQ methods** that are best suited for integration within the project's modelling and simulation activities, and which align with emerging trends in machine learning and data-driven modelling.
- **Initiate the characterization of uncertainties** associated with hydrogen-powered propulsion architectures by mapping sources of uncertainty across components and lifecycle phases.
- **Foster collaboration** across work packages by summarizing inputs and perspectives from experimental, modelling, and systems-level partners, with the goal of converging on a unified approach to uncertainty management.

This deliverable marks a first step in WP3's objective to develop innovative uncertainty quantification strategies tailored to the needs of next-generation sustainable aviation technologies and will serve as a reference point for future deliverables and technical integration across the project. Developed with input from all work packages, this deliverable is intended as a dynamic document that will continue to evolve as the project progresses.

## 1.2. Structure of the document

The structure of the document is outlined below and is organized into the following four chapters:

- **Chapter 1** introduces this deliverable.
- **Chapter 2** outlines the role of uncertainty quantification and the associated challenges in engineering design.
- **Chapter 3** presents a review of state-of-the-art UQ techniques, including sampling-based approaches, surrogate modelling, and multi-fidelity strategies.
- **Chapter 4** provides an initial analysis of the sources and nature of uncertainty across hydrogen-powered propulsion components. It considers the fidelity of available models and the relevance of uncertainty at various stages of the system lifecycle, incorporating contributions from multiple work packages.

## 2. Engineering design under uncertainty

This section presents the fundamentals of uncertainty quantification, a core element underpinning all work packages within the DEMOQUAS project. It outlines the key concepts involved, introduces the principle of uncertainty propagation, and then explores its various applications and associated challenges.

### 2.1. Uncertainty quantification and propagation

Modern engineering increasingly relies on simulations and data-driven models to make decisions during design and analysis. However, all models involve some level of uncertainty, whether from variability in material properties, operating conditions, or incomplete knowledge of complex systems. Uncertainty quantification is the field that deals with identifying, understanding, and managing these uncertainties to make better, more reliable decisions. It is an interdisciplinary field bridging statistics, computer science, and engineering, focused on identifying, characterizing, and reducing uncertainties throughout design, manufacturing, and operational processes. Within predictive engineering science, it involves assessing the uncertainty and potential errors in models, simulations, and experimental data. This field plays a vital role in enhancing the reliability of predictions by addressing the various sources of uncertainty. Uncertainty is typically categorized into two types: aleatoric and epistemic<sup>1</sup>. Aleatoric uncertainty stems from inherent randomness or variability in the data, while epistemic uncertainty arises from incomplete knowledge or limited understanding of the underlying processes. Accounting for both types allows for a more comprehensive estimation of a model's accuracy in representing real-world behaviour.

During the modelling, simulation, and design stages, uncertainties arise from the selection of physical models and the specification of input parameters necessary for analysis. Uncertainty quantification frameworks typically address these uncertainties by first quantifying the input uncertainty and then propagating it through the model to assess its impact on the outputs<sup>2</sup>. As illustrated in Figure 1, this process begins by characterizing the uncertainty in the input variables, commonly represented by probability distributions. The model is then evaluated using multiple random samples drawn from these distributions, ultimately resulting in a statistical approximation of the output uncertainty. In this approach commonly referred to as the Monte Carlo method<sup>3</sup>,

---

<sup>1</sup> Box, G. E. P., and Draper, N. R., "Empirical Model-Building and Response Surfaces," Wiley, New York, 1987.

<sup>2</sup> Roy, C. J., and Oberkampf, W. L., "A Comprehensive Framework for Verification, Validation, and Uncertainty Quantification in Scientific Computing," *Computer Methods in Applied Mechanics and Engineering*, vol. 200, nos. 25–28, 2011, pp. 2131–2144.

<sup>3</sup> Hammersley, J. M., and Handscomb, D. C., "Monte Carlo Methods," Springer Netherlands, Dordrecht, 1964.

the model is considered a black-box and the framework is non-intrusive. In practice, the brute force Monte Carlo method is rarely used on its own because it requires a large number of model evaluations to achieve a reliable approximation of output uncertainty, which can be computationally expensive.

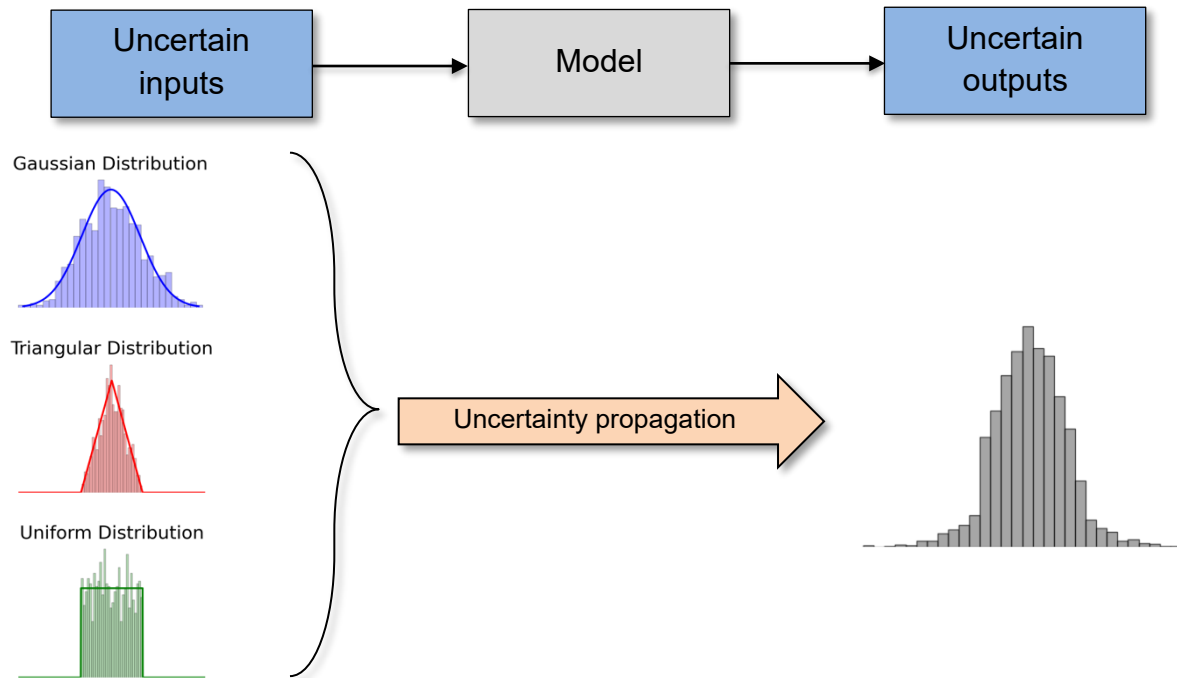


**Figure 1.** Representation of uncertainty propagation using Monte Carlo sampling, where the uncertain inputs are drawn from Gaussian, triangular, and uniform distributions.

## 2.2. Applications in industry

Modelling and simulation are essential tools for the design and development of engineering systems across industries, including aerospace. They play a critical role in the design and development phases of aerospace engineering by enabling the analysis and prediction of complex system behaviours without the need for costly physical prototypes. They support decision-making by providing insights into performance, safety, and reliability under various operating conditions. These tools are essential for optimizing designs, reducing development time, and managing risk throughout the engineering process. Uncertainty quantification intervenes in the latter by systematically accounting for variability and incomplete knowledge in inputs, models, and conditions. By quantifying the impact of these uncertainties on simulation results, it supports more robust, reliable, and risk-informed design decisions. Uncertainty quantification applications in industry can be divided into four categories:

1. Uncertain predictions: involve capturing and modelling inherent randomness in system inputs or environmental conditions, such as material properties, loads, or temperature fluctuations, and propagating this uncertainty through simulations to estimate its effect on performance or safety.
2. Reliability analysis: assess the probability of failure or performance degradation by computing how likely it is that a system will meet its requirements under uncertain conditions, helping to ensure safety and compliance with design standards.
3. Sensitivity analysis: identify which input parameters have the most significant impact on the system's output, guiding engineers to focus on the most influential factors and prioritize data collection or model refinement where it matters most.
4. Robust design: support the development of designs that maintain consistent performance despite variations in operating conditions or input uncertainties, leading to more dependable and resilient engineering solutions.

In summary, uncertainty quantification is a vital component of modern engineering design and analysis, enabling more reliable predictions, safer systems, and better-informed decisions. By systematically addressing variability and lack of knowledge, uncertainty quantification strengthens the role of modelling and simulation within the design and development phases. However, uncertainty quantification remains a relatively recent and evolving field that must overcome several challenges before it can be fully embedded into standard engineering design processes.

### 2.3. Challenges in applying uncertainty quantification

Despite well-established theoretical foundations and successful applications in both research and industry, applying uncertainty quantification to real-world engineering problems remains challenging. Several practical obstacles can limit its effectiveness, including<sup>4</sup>:

1. Limited data availability: accurately inferring input probability distributions requires sufficient data, but in industrial settings, time and cost constraints often limit data availability. As a result, distribution construction relies heavily on assumptions, introducing subjectivity and potential errors that are frequently underestimated.

---

<sup>4</sup> Ahlfeld, R. "A data-driven uncertainty quantification method for scarce data and rare events." PhD diss., Imperial College London, 2017.

2. Curse of dimensionality: analysing complex systems often involves exploring high-dimensional design spaces, where the number of uncertain parameters is large. This significantly increases the data and computational effort required for reliable uncertainty quantification, making its application challenging and sometimes impractical.
3. Estimating rare events: statistical assumptions, such as modelling inputs with a Gaussian distribution, often fail to capture rare but possible events that lie in the tails of the distribution. These low-probability occurrences, known as Black Swans, can have disproportionately large and unforeseen impacts, making their omission particularly critical in risk-sensitive applications.
4. Model discontinuities: some computational models exhibit discontinuities or sharp gradients, stemming from strong nonlinearities in the underlying equations. A common example is compressible flow simulations, where shock waves create abrupt changes in solution behaviour. Such features can hinder the accuracy and efficiency of uncertainty quantification methods, which typically assume smoother, more regular model responses.
5. Model-form uncertainty: both models based on partial differential equations and surrogate models rely on simplifying assumptions and approximations, introducing epistemic uncertainty. This type of uncertainty is often difficult to quantify accurately and poses additional challenges when combining it with other sources of uncertainty, such as inherent variability in input parameters.

Although not exhaustive, addressing these key challenges is crucial for advancing the practical adoption of uncertainty quantification, making it more accessible, computationally efficient, and seamlessly integrated into industrial design and decision-making processes.

### 3. Uncertainty quantification methods

Uncertainty quantification methods provide a structured approach to assess how uncertainties in model inputs affect outputs. These methods can generally be divided into two categories: deterministic and probabilistic. Deterministic approaches typically explore the bounds of uncertainty using worst-case scenarios or interval analysis. In contrast, probabilistic methods treat uncertainty through statistical modelling, using probability distributions to represent input variability and propagate it through the model. This section focuses on probabilistic uncertainty quantification methods, which are especially effective for capturing complex, data-driven uncertainties commonly encountered in modern engineering challenges. It will examine three key categories of techniques: pseudo-random sampling methods for direct uncertainty propagation, surrogate-based approaches that approximate complex models to reduce computational cost, and multi-fidelity strategies that combine models of varying accuracy to efficiently balance precision and performance.

#### 3.1. Pseudo-random sampling methods

Pseudo-random sampling methods are among the most widely used techniques for uncertainty propagation, as they require minimal assumptions about the quantity of interest or the structure of the model. Given a random vector  $X$  distributed according to some probability distribution  $\Pi$ , random sampling would ideally involve drawing  $N$  independent and identically distributed realizations  $\{X_i\}$  from  $\Pi$ . However, true random sampling is computationally infeasible in practice. Instead, we use pseudo-random sampling, where a sequence  $\{X_i(\omega)\}$  is generated to approximate samples from  $\Pi$  using deterministic algorithms designed to mimic randomness, ensuring the samples are uncorrelated and statistically representative. These algorithms typically begin by generating values from the standard uniform distribution  $U([0, 1))$  and then apply transformation techniques to map those values onto the desired target distribution.

#### Monte Carlo method

The goal of the Monte Carlo method is to approximate the distribution of a parameterized quantity of interest function  $f$  by generating a collection of sample evaluations  $\{f(X_i)\}$ , where the input vector  $X$  follows a known probability distribution  $\Pi$ . Given such a function  $f$ , a distribution  $\Pi$ , and a random number generator for  $X$ , the method involves three main steps:

1. Generate  $N$  independent and identically distributed samples  $\{X_j(\omega)\}$  from the distribution  $\Pi$  using the random number generator.

2. Evaluate the function on each sample to obtain  $\{f(X_j(\omega))\}$  as represented in Figure 1.
3. Use these function evaluations  $\{f(X_j(\omega))\}$  to characterize the behaviour of  $f$ , typically by calculating statistical measures such as the mean, variance, or applying other techniques to characterize the resulting empirical distribution.

This approach relies on the definition of the sample mean,

$$E[f] = \mu_f \approx \bar{\mu}_f = \frac{1}{N} \sum_{i=1}^N f(X_i)$$

and is grounded in the Central Limit Theorem, which guarantees that the distribution of the sample mean converges to a normal distribution as the number of samples  $N$  increases. However, the convergence rate of the method is relatively slow compared to that of typical numerical algorithms, which significantly limits its practicality and accuracy, especially when evaluating the function  $f$  is computationally costly.

## Latin Hypercube

The convergence of estimated moments of  $f$  to their exact values is often quite slow, largely due to the low quality and slow convergence of the sample ensemble  $\{X_j(\omega)\}$  toward the target distribution  $X$ . Latin Hypercube Sampling<sup>5</sup> improves the quality of the sample set, often resulting in faster convergence of the estimators. While the evaluation steps remain the same as in the standard Monte Carlo method, the way the sample ensemble is constructed differs:

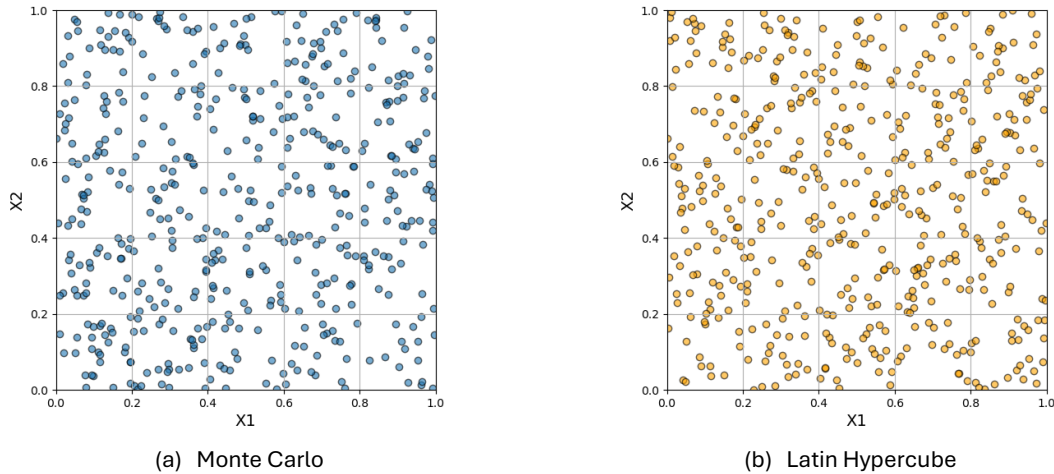
1. Assuming  $X \sim U([0, 1]^d)$ , each of the  $d$  dimensions is divided into  $N$  intervals, forming  $N^d$  cells.
2. The  $N$  samples are then selected such that each one occupies a unique cell, ensuring no two samples share the same interval along any dimension.

Figure 2 compares two sampling strategies in a two-dimensional space: uniform random sampling (left) and Latin Hypercube Sampling (right). Once the uniform samples

---

<sup>5</sup> McKay M. D., Beckman R. J., and Conover W. J. "A Comparison of Three Methods for Selecting Values of Input Variables in the Analysis of Output from a Computer Code." *Technometrics*, vol. 42, no. 1, 2000, pp. 55–61.

are generated, they can be transformed into samples from more complex distributions using methods such as the inverse transform.



**Figure 2.** Monte Carlo and Latin Hypercube samples of  $X \sim U([0,1]^2)$ .

### 3.2. Surrogate-based methods

In uncertainty quantification, the physical or computational model of a system is often treated as a black box that defines a mapping:

$$Y = f(\mathbf{X}),$$

where  $\mathbf{X}$  is a random vector representing the uncertainty in input parameters, typically characterised by a joint probability density function, and  $Y$  is the resulting random variable describing the model's output response. Direct approaches like Monte Carlo simulation, as discussed earlier, often require running the computational model thousands or even millions of times for different realisations  $\{X_i\}$  of the input random variable. However, in many applied science and engineering contexts (such as high-fidelity finite element or computational fluid dynamics models) each simulation can be extremely computationally expensive. As a result, such direct methods become impractical. To address this challenge, surrogate models have become a fundamental tool in uncertainty quantification, offering a more efficient alternative by approximating the original model at a fraction of the computational cost.

A surrogate model  $\hat{f}$  is a computationally efficient approximation of the true model, expressed as  $f(\mathbf{X}) = \hat{f}(\mathbf{X}; \theta) + \varepsilon$ , where  $\theta$  denotes the set of parameters defining the surrogate and  $\varepsilon$  represents the approximation error. These parameters are typically determined through an optimisation process using a limited number of evaluations of the

original model, known as the design of experiment, consisting of input samples  $\{x_1, \dots, x_N\}$ . This deliverable introduces three families of surrogate models, with more comprehensive coverage and detailed discussions available in the broader literature<sup>6,7</sup>.

## Gaussian processes

Gaussian processes are well established in the statistics and machine learning community<sup>8</sup>. They represent distributions over functions written as  $f: \mathbf{X}_i \in \mathcal{D} \rightarrow f(\mathbf{X}_i) \in \mathbb{R}$  which associate an input vector  $\mathbf{X}_i \in \mathcal{D}$  on the design space  $\mathcal{D} \in \mathbb{R}^d$  of dimension  $d$  with a scalar output quantity  $f$ . Noisy observations are often considered and written as  $y(\mathbf{X}_i) = f(\mathbf{X}_i) + \epsilon$  with the noise being an independent and identically distributed Gaussian variable  $\epsilon$  with zero mean and variance  $\tau^2$ . Let  $\mathbf{X} = [\mathbf{X}_1, \dots, \mathbf{X}_N]$  be the matrix of  $N$  training points and  $\mathbf{f} = f(\mathbf{X}) = [f_1, \dots, f_N]^\top$  the latent variable vector. The observable variable vector is defined in the same way,  $\mathbf{y} = y(\mathbf{X}) = [y_1, \dots, y_N]^\top$ . The main idea behind Gaussian processes is that the values of  $\mathbf{y}$  are jointly Gaussian with mean  $m(\mathbf{X})$  and covariance  $k(\mathbf{X}, \mathbf{X})$  where  $m$  is the mean function and  $k$  is the covariance function.

A Gaussian process is characterised by the mean function and the covariance function. Since it holds for any set on the design space, it includes the set containing the training points  $\mathbf{X}$  and a test point  $\mathbf{X}^*$ . Then,  $f(\mathbf{X}^*)$  can be inferred by manipulating the joint Gaussian distribution. For all test points  $\mathbf{X}^*$ , the Gaussian process prior,  $p(\mathbf{y}, \mathbf{f}^*)$ , can be written as a joint normal distribution over the random variable vectors  $\mathbf{y}$  and  $\mathbf{f} = f(\mathbf{X}^*)$ ,

$$p(\mathbf{y}, \mathbf{f}^*) = \mathcal{N} \left( \begin{bmatrix} m(\mathbf{X}) \\ m(\mathbf{X}^*) \end{bmatrix}, \begin{bmatrix} k(\mathbf{X}, \mathbf{X}) + \tau^2 & k(\mathbf{X}, \mathbf{X}^*) \\ k(\mathbf{X}^*, \mathbf{X}) & k(\mathbf{X}^*, \mathbf{X}^*) \end{bmatrix} \right).$$

To make predictions of the function outputs,  $\mathbf{f}^* = f(\mathbf{X}^*)$  the posterior distribution  $p(\mathbf{f}^* | \mathbf{X}^*, \mathbf{X}, \mathbf{y})$  can be derived by applying the multivariate Gaussian conditional rule which gives  $p(\mathbf{f}^* | \mathbf{X}^*, \mathbf{X}, \mathbf{y}) = \mathcal{N}(\mathbf{f}^* | \mu_{GP}(\mathbf{X}^*), \sigma_{GP}(\mathbf{X}^*))$  with posterior mean  $\mu_{GP}$  and posterior standard deviation  $\sigma_{GP}$  defined as:

$$\begin{aligned} \mu_{GP}(\mathbf{X}^*) &= m(\mathbf{X}^*) + k(\mathbf{X}^*, \mathbf{X})[k(\mathbf{X}, \mathbf{X}) + \tau^2]^{-1}(\mathbf{y} - m(\mathbf{X})), \\ \sigma_{GP}(\mathbf{X}^*) &= k(\mathbf{X}^*, \mathbf{X}^*) - k(\mathbf{X}^*, \mathbf{X})[k(\mathbf{X}, \mathbf{X}) + \tau^2]^{-1}k(\mathbf{X}, \mathbf{X}^*). \end{aligned}$$

<sup>6</sup> Montomoli, F., Ed., "Uncertainty Quantification in Computational Fluid Dynamics and Aircraft Engines," Springer International Publishing, 2019.

<sup>7</sup> Smith, R. C., "Uncertainty Quantification: Theory, Implementation, and Applications," SIAM, Society for Industrial and Applied Mathematics, 2024.

<sup>8</sup> Rasmussen, C. E. and Williams, C., "Gaussian Processes for Machine Learning", The MIT Press, 2006.

The standard deviation,  $\sigma_{GP}$ , quantifies the uncertainty arising from the approximation process and corresponds to the uncertainty in the model prediction away from a training point. The posterior distribution strongly depends on the formulations used for  $m(\mathbf{X})$  and covariance  $k(\mathbf{X}, \mathbf{X})$ . Whereas the mean function is commonly assumed to be zero on the design space,  $m(\mathbf{X}) = 0$ , the covariance function incorporates the function's structure available under the Gaussian process prior. In other words, it determines the properties of the resulting Gaussian process model. Thus, the flexibility provided by Gaussian process regression is counterbalanced by the necessity to choose this covariance function that best suits the structure of the training data and to find its most optimal parameters. Figure 3 shows an example of Gaussian process applied to one-dimensional data. Further information on the covariance function and the training of Gaussian processes is available in the existing literature<sup>8</sup>.

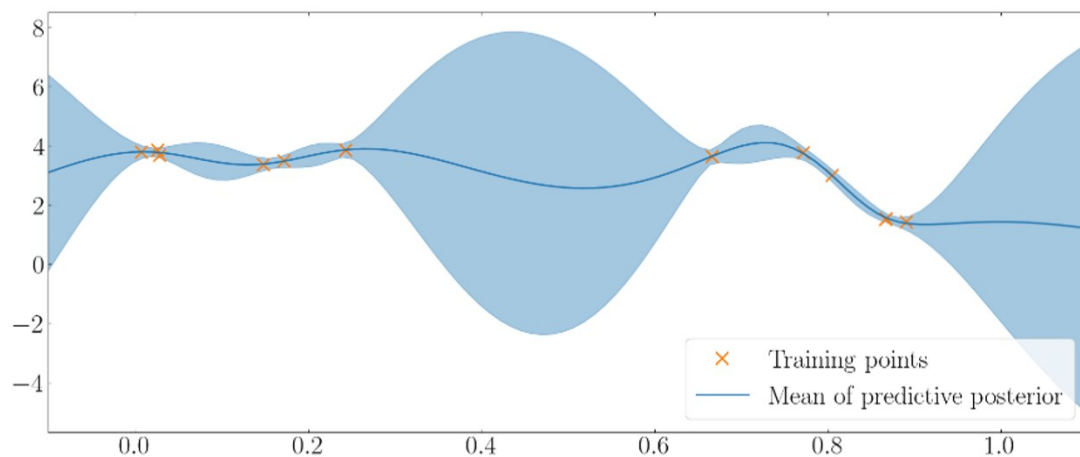


**Figure 3.** Gaussian process example with representative mean and confidence interval.

Gaussian Processes have become a widely adopted tool for uncertainty quantification in aerospace design. For instance, in aerodynamic shape optimisation, Gaussian processes are commonly used to emulate expensive computational fluid dynamics simulations, enabling efficient design space exploration and global optimisation under uncertainty<sup>9,10</sup>. They have also been applied in structural reliability analysis to estimate rare event probabilities and assess performance under load variability<sup>11,12</sup>. In the domain of aircraft engines and propulsion systems, Gaussian

<sup>9</sup> Forrester, A. I. J., Sobester, A., & Keane, A. J., "Engineering Design via Surrogate Modelling: A Practical Guide", Wiley, 2008.

<sup>10</sup> Toal, D. J. J., "Some Considerations Regarding the Use of Multi-Fidelity Kriging in the Construction of Surrogate Models," Structural and Multidisciplinary Optimization, Vol. 51, No. 6, 2015, pp. 1223–1245.

<sup>11</sup> Bichon, B. J., Eldred, M. S., Swiler, L. P., Mahadevan, S., and McFarland, J. M., "Efficient Global Reliability Analysis for Nonlinear Implicit Performance Functions," AIAA Journal, Vol. 46, No. 10, 2008, pp. 2459–2468.

<sup>12</sup> Echard, B., Gayton, N., and Lemaire, M., "AK-MCS: An Active Learning Reliability Method Combining Kriging and Monte Carlo Simulation," Structural Safety, Vol. 33, No. 2, 2011, pp. 145–154.

processes were used to estimate the aircraft fuel flow rate<sup>13</sup> and to quantify the uncertainty of the performance of a typical turboshaft engine<sup>14</sup>.

## Polynomial chaos expansions

Polynomial Chaos Expansions (PCE) are a spectral method for representing uncertainty in mathematical models by expanding a model's output as a series of orthogonal polynomials of the input random variables<sup>15,16</sup>. The key idea is to express the response of a system with uncertain inputs as a weighted sum of polynomial basis functions that are orthogonal with respect to the probability distribution of those inputs. Suppose  $\mathbf{X} = (X_1, X_2, \dots, X_d)$  is a vector of  $d$  independent random variables with known distributions and let  $Y = f(\mathbf{X})$  be the model output. The PCE approximates  $Y$  as a linear combination of  $N_P$  stochastic multivariate orthogonal polynomials:

$$\hat{Y}(\mathbf{X}) = \sum_{k=1}^{N_P} \alpha_k \cdot \Psi_k(\mathbf{X})$$

where  $\Psi_k(\mathbf{X})$  are multivariate orthogonal polynomial basis functions and each of them is a production of univariate polynomials  $\psi_{k_i}(X_i)$ . This approach transforms the problem of uncertainty quantification into the computation of the coefficients  $\alpha_k$  of the expansion, which can be done through regression, projection, or sampling-based techniques. Different families of orthogonal polynomials serve as optimal basis functions in Polynomial Chaos Expansions, depending on the input probability distribution. For instance, Hermite polynomials are suited for Gaussian-distributed inputs, Legendre polynomials for uniform distributions, and Laguerre polynomials for exponential distributions.

Over the years, several variants of PCE have been developed to overcome limitations of the original formulation and to broaden its applicability in engineering contexts. The classical PCE was initially restricted to Gaussian inputs using Hermite polynomials<sup>17</sup>. This was later extended through the Generalized Polynomial Chaos framework<sup>16</sup>, which incorporates orthogonal polynomials matched to various input distributions, such as

<sup>13</sup> Chati, Y. S., and Balakrishnan, H., "A Gaussian Process Regression Approach to Model Aircraft Engine Fuel Flow Rate," Proceedings of the 8th ACM/IEEE International Conference on Cyber-Physical Systems, Pittsburgh, PA USA, April 2017.

<sup>14</sup> Liu, X., Tang, H., Zhang, X., and Chen, M., "Gaussian Process Model-Based Performance Uncertainty Quantification of a Typical Turboshaft Engine," Applied Sciences, Vol. 11, No. 18, 2021, p. 8333.

<sup>15</sup> Ghanem, R. G., and Spanos, P. D., "Stochastic Finite Elements: A Spectral Approach," Springer New York, New York, NY, 1991.

<sup>16</sup> Xiu, D., and Karniadakis, G. E., "The Wiener--Askey Polynomial Chaos for Stochastic Differential Equations," SIAM Journal on Scientific Computing, Vol. 24, No. 2, 2002, pp. 619--644.

<sup>17</sup> Wiener, N., "The Homogeneous Chaos," American Journal of Mathematics, Vol. 60, No. 4, 1938, p. 897.

Legendre for uniform and Laguerre for exponential inputs. To address high-dimensional problems, sparse PCE techniques were introduced<sup>18</sup>, leveraging compressive sensing and LASSO-type regression methods to retain only the most influential terms. Adaptive PCE approaches dynamically refine the polynomial basis or truncation strategy based on error estimates or convergence criteria<sup>19</sup>. Furthermore, non-intrusive formulations treat the model as a black box and rely solely on input-output evaluations, making them highly suitable for industrial applications. The Arbitrary PCE extends traditional chaos expansion methods to handle arbitrary input distributions with arbitrary probability measures<sup>20</sup>. These measures may be discrete, continuous, or discretised forms of continuous distributions, and can be specified in various ways, analytically through probability density or cumulative distribution functions, numerically as histograms, or directly from raw data samples.

## Neural networks

Deep learning is a subset of machine learning, inspired by the structure and function of the human brain's neural network<sup>21</sup>. It provides solutions to complex tasks by automatically learning hierarchical representations of data. Deep neural networks consist of multiple layers (deep layers) of interconnected artificial neurons, which process and transform input data. These networks are trained on large data sets, adjusting their internal parameters through a process known as backpropagation to minimise prediction errors. Mathematically, deep neural network is a composite function that learns to approximate complex mappings between input and output data by composing multiple layers of transformations, each driven by learnable parameters. Each layer in a deep neural network transforms its input through a series of linear and non-linear operations, gradually learning hierarchical representations of the input data.

Let  $\mathbf{X}$  denote the input to the network,  $\mathbf{h}^l$  denote the output of the  $l$ -th layer, and  $\mathbf{W}^l$  and  $\mathbf{b}^l$  denote the matrix of weights and the vector of biases of layer  $l$ , respectively. The output of each layer is computed as follows:

$$\mathbf{h}^l = \varphi^l(\mathbf{W}^l \mathbf{h}^{l-1} + \mathbf{b}^l)$$

<sup>18</sup> Blatman, G., and Sudret, B., "Adaptive Sparse Polynomial Chaos Expansion Based on Least Angle Regression," *Journal of Computational Physics*, Vol. 230, No. 6, 2011, pp. 2345–2367.

<sup>19</sup> Wan, X., and Karniadakis, G. E., "Multi-Element Generalized Polynomial Chaos for Arbitrary Probability Measures," *SIAM Journal on Scientific Computing*, Vol. 28, No. 3, 2006, pp. 901–928.

<sup>20</sup> Oladyskhin, S., and Nowak, W., "Data-Driven Uncertainty Quantification Using the Arbitrary Polynomial Chaos Expansion," *Reliability Engineering & System Safety*, Vol. 106, 2012, pp. 179–190.

<sup>21</sup> Bishop, C. M., and Bishop, H., "Deep Learning," Springer, 2024.

where  $\varphi$  is the activation function applied elementwise to the weighted sum of inputs. A multilayer perceptron, also called fully connected neural network or feedforward neural network, consists of  $L$  layers of interconnected neurons, typically including an input layer, one or more hidden layers, and an output layer. Formally, it is written:

$$f(\mathbf{X}, \boldsymbol{\theta}) = \mathbf{W}^L \varphi^{L-1}(\mathbf{W}^{L-1} \varphi^{L-2} (\dots \varphi^1(\mathbf{W}^1 \mathbf{X})))$$

where  $\boldsymbol{\theta}$  contains the parameters, the biases being included in the matrices  $\mathbf{W}$ . During the training phase of the neural network, the goal is to adjust the parameters of  $\boldsymbol{\theta}$  the network in such a way that the network learns to map inputs to outputs effectively. This is achieved through minimising a loss function, which measures the discrepancy between the predicted outputs of the network and the true labels associated with the input data.

The multilayer perceptron, as shown in Figure 4, is one of the earliest and simplest forms of neural network architectures. Despite its simplicity, it laid the foundation for modern neural networks by demonstrating the ability to approximate complex functions. Modern deep learning architectures, such as convolutional neural networks, recurrent neural networks, transformers, and graph neural networks, have significantly expanded upon this basic structure. These advanced models incorporate specialised components like attention mechanisms, recurrence, or convolutional layers, enabling them to learn intricate patterns and dependencies in data across a wide range of domains, from image recognition and natural language processing to scientific computing.

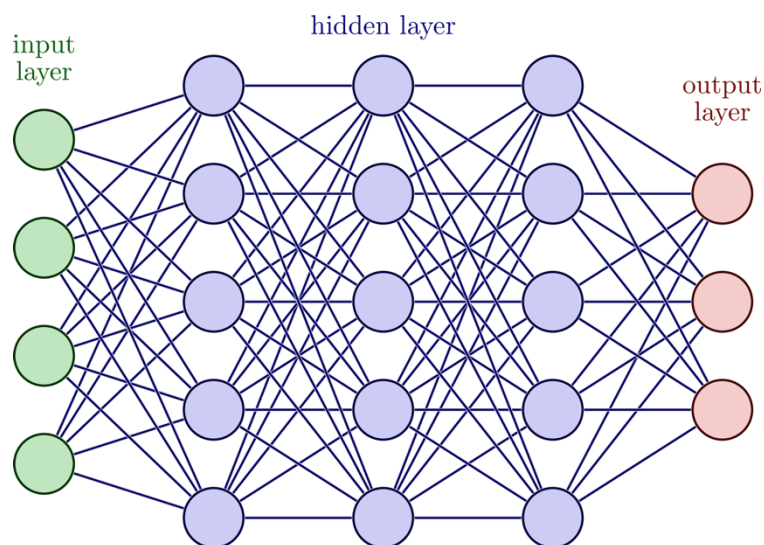


**Figure 4.** Example of multilayer perceptron with three hidden layers.

Deep learning has gained traction as a surrogate modelling tool in uncertainty quantification, offering scalability and flexibility in approximating complex, nonlinear systems in computational science and engineering. Unlike traditional methods, such as polynomial chaos or Gaussian processes, deep neural networks can effectively handle high-dimensional input spaces and large datasets, making them particularly well-suited for computationally intensive simulations. For example, in the field of chemistry, neural networks were used to incorporate uncertainty quantification into molecular design<sup>22</sup> and the prediction of molecular properties<sup>23</sup>. In fluid dynamics, encoder-decoder networks were employed to create deep surrogates for stochastic partial differential equations, enabling efficient forward uncertainty propagation in porous media flow<sup>24</sup>. In structural mechanics, surrogates based on generative models were integrated within uncertainty quantification pipelines for efficient probabilistic failure analysis<sup>25</sup>. Another trend involves integrating domain knowledge through physics-informed neural networks, which embed governing equations directly into the loss function. This approach has been used for uncertainty propagation in the flight dynamic of a simulated combat aircraft<sup>26</sup>. A more comprehensive review of deep learning applications in the uncertainty quantification of engineering systems is available in the literature<sup>27</sup>.

### 3.3. Multi-fidelity methods

The core idea behind multi-fidelity methods is that, throughout the engineering design and development process, a range of simulation tools and models are employed, each varying in fidelity, accuracy, and computational cost. These methods aim to estimate a quantity of interest by combining information from both low-fidelity (e.g., empirical models or coarse simulations) and high-fidelity (e.g., high-resolution CFD or finite element models) sources. For example, in CFD, potential flow models may serve as low-fidelity tools, while Reynolds-averaged Navier–Stokes simulations provide high-fidelity data. By strategically leveraging the strengths of each model, multifidelity approaches

---

<sup>22</sup> Chen, L.Y., Li, Y.P., “Uncertainty quantification with graph neural networks for efficient molecular design”, *Nature Communications*, Vol. 16, 2025, p. 3262.

<sup>23</sup> Yang, C.-I., and Li, Y.-P., “Explainable Uncertainty Quantifications for Deep Learning-Based Molecular Property Prediction,” *Journal of Cheminformatics*, Vol. 15, No. 1, 2023, p. 13.

<sup>24</sup> Zhu, Y., and Zabarar, N., “Bayesian Deep Convolutional Encoder–Decoder Networks for Surrogate Modelling and Uncertainty Quantification,” *Journal of Computational Physics*, Vol. 366, 2018, pp. 415–447.

<sup>25</sup> Silionis, N. E., Liangou, T., and Anyfantis, K. N., “Deep Learning-Based Surrogate Models for Spatial Field Solution Reconstruction and Uncertainty Quantification in Structural Health Monitoring Applications,” *Computers & Structures*, Vol. 301, 2024, p. 107462.

<sup>26</sup> Michek, N., Mehta, P., and Huebsch, W., “Flight Dynamic Uncertainty Quantification Modelling Using Physics-Informed Neural Networks,” Orlando, FL, 2024.

<sup>27</sup> Shi, Y., Wei, P., Feng, K., Feng, D.-C., and Beer, M., “A Survey on Machine Learning Approaches for Uncertainty Quantification of Engineering Systems,” *Machine Learning for Computational Science and Engineering*, Vol. 1, No. 1, 2025, p. 11.

enable more efficient and accurate uncertainty quantification than would be possible using high-fidelity simulations alone<sup>28,29</sup>.

One of the earliest strategies is the multifidelity Monte Carlo approach<sup>30</sup>. For instance, it has been applied to robust wing optimization problems, where the approach strategically distributes computational effort between high- and low-fidelity models, taking into account their respective evaluation costs and the degree of correlation between their outputs<sup>31</sup>. It is also employed in the uncertainty quantification of heat transfer within a rectangular ribbed channel by using fine and coarse CFD meshes to represent the high- and low-fidelity models, respectively<sup>32</sup>. Building on these ideas, multifidelity extensions of Polynomial Chaos Expansions have also been developed. For instance, stochastic collocation methods were adapted to leverage multifidelity models<sup>33,34</sup>. More recently, neural networks have been adapted to multifidelity contexts, which show how they can flexibly model nonlinear correlations between fidelity levels for uncertainty quantification tasks. The idea involves constructing composite neural networks in which a low-fidelity model is first trained, and its output is subsequently refined using high-fidelity data<sup>35</sup>. Such architecture was applied to model the physical flow inside an aircraft propulsion system while accounting for aleatory uncertainties originating from experimental measurement errors<sup>36</sup>. In line with the principles of multifidelity methods that incorporate models of varying accuracy, data fusion combines computational models with experimental data to enhance the reliability and accuracy of predictions<sup>37,38</sup>. Although multifidelity methods are commonly used in uncertainty quantification, the integration of evidence from both computational models and experimental data to enhance uncertainty propagation has received comparatively less attention.

<sup>28</sup> Kennedy, M. and O'Hagan, A., "Predicting the Output from a Complex Computer Code When Fast Approximations Are Available," *Biometrika*, Vol. 87, No. 1, 2000, pp. 1–13.

<sup>29</sup> Peherstorfer, B., Willcox, K., and Gunzburger, M., "Survey of Multifidelity Methods in Uncertainty Propagation, Inference, and Optimization," *SIAM Review*, Vol. 60, No. 3, 2018, pp. 550–591.

<sup>30</sup> Giles, M. B., "Multilevel Monte Carlo Path Simulation," *Operations Research*, Vol. 56, No. 3, 2008, pp. 607–617.

<sup>31</sup> Ng, L. W. T., and Willcox, K. E., "Multifidelity Approaches for Optimization under Uncertainty", *International Journal for Numerical Methods in Engineering*, Vol. 100, No. 10, 2014, pp. 746–772.

<sup>32</sup> Doostan, A., Geraci, G., and Iaccarino, G., "A Bi-Fidelity Approach for Uncertainty Quantification of Heat Transfer in a Rectangular Ribbed Channel," *ASME Turbo Expo 2016*, Seoul, South Korea, 2016.

<sup>33</sup> Narayan, A., Gittelson, C., and Xiu, D., "A Stochastic Collocation Algorithm with Multifidelity Models," *SIAM Journal on Scientific Computing*, Vol. 36, No. 2, 2014, pp. A495–A521.

<sup>34</sup> Palar, P. S., Tsuchiya, T., and Parks, G. T., "Multi-Fidelity Non-Intrusive Polynomial Chaos Based on Regression," *Computer Methods in Applied Mechanics and Engineering*, Vol. 305, 2016, pp. 579–606.

<sup>35</sup> Meng, X., and Karniadakis, G. E., "A Composite Neural Network That Learns from Multi-Fidelity Data: Application to Function Approximation and Inverse PDE Problems," *Journal of Computational Physics*, Vol. 401, 2020, p. 109020.

<sup>36</sup> Li, Z., and Montomoli, F., "Aleatory Uncertainty Quantification Based on Multi-Fidelity Deep Neural Networks," *Reliability Engineering & System Safety*, Vol. 245, 2024, p. 109975.

<sup>37</sup> Bertram, A., Bekemeyer, P., and Held, M., "Fusing Distributed Aerodynamic Data Using Bayesian Gappy Proper Orthogonal Decomposition," *AIAA Aviation Forum*, Virtual event, 2021.

<sup>38</sup> Feldstein, A., Lazzara, D., Princen, N., and Willcox, K., "Multifidelity Data Fusion: Application to Blended-Wing-Body Multidisciplinary Analysis Under Uncertainty," *AIAA Journal*, Vol. 58, No. 2, 2020, pp. 889–906.

### 3.4. Sensitivity analysis

The goal of sensitivity analysis is to identify the parameters which give the biggest contribution to the uncertainty of a system's output. While uncertainty propagation focuses on characterizing the distribution of the output  $Y$ , sensitivity analysis seeks to assess and quantify how much each input variable  $X_i$ , or groups of inputs, contribute to the variability of  $Y$ .

Sensitivity analysis methods are commonly categorized into local and global approaches. Local sensitivity analysis evaluates the effect of small perturbations around a nominal value of the input variables, typically using partial derivatives. It is simple to implement and computationally inexpensive but provides limited insight, especially for nonlinear or highly uncertain systems, since it only captures behaviour near a specific point. In contrast, global sensitivity analysis considers the entire input space, taking into account the full range of variability in the inputs. These techniques provide a more comprehensive understanding of how inputs influence the output, including interaction effects. Although more computationally demanding, global methods offer a more robust picture of model behaviour under uncertainty.

#### Challenges

Sensitivity analysis is typically carried out through sampling-based methods<sup>39</sup>, which involve running the model repeatedly. While this approach is broadly applicable, it presents several challenges in practice:

- Computational cost: High-fidelity or complex models, such as those involving computational fluid dynamics or finite element analysis, often have expensive evaluation times. Performing a large number of runs to explore sensitivity becomes computationally prohibitive.
- High-dimensional input spaces: As the number of uncertain input parameters increases, the dimensionality of the input space grows, a phenomenon known as the curse of dimensionality. This drastically increases the number of required simulations to achieve accurate sensitivity estimates<sup>40</sup>.
- Input correlations: Many sensitivity analysis methods assume that inputs are statistically independent. However, in realistic engineering problems, inputs are

---

<sup>39</sup> Helton, J. C., Johnson, J. D., Sallaberry, C. J., and Storlie, C. B., "Survey of Sampling-Based Methods for Uncertainty and Sensitivity Analysis," *Reliability Engineering & System Safety*, Vol. 91, Nos. 10–11, 2006, pp. 1175–1209.

<sup>40</sup> Tsvetkova, O., and Ouarda, T. B. M. J., "Quasi-Monte Carlo Technique in Global Sensitivity Analysis of Wind Resource Assessment with a Study on UAE," *Journal of Renewable and Sustainable Energy*, Vol. 11, No. 5, 2019, p. 053303.

often correlated. Ignoring these correlations can lead to misleading sensitivity measures, necessitating advanced techniques that can account for dependency structures<sup>41</sup>.

- Nonlinear model responses: Methods based on linear assumptions can underestimate or misrepresent sensitivity when the model output exhibits nonlinear behaviour with respect to its inputs.
- Multi-output models: While sensitivity analysis is traditionally developed for scalar outputs, many models yield vector-valued or functional outputs<sup>42</sup>. In such cases, separate analyses can be performed for each output, but interpreting sensitivity across correlated outputs remains complex and may require dimension reduction or multivariate sensitivity frameworks.
- Stochastic models: In some models, repeated runs with the same input parameters yield different outputs due to intrinsic randomness. For such cases, it is important to distinguish the variability caused by the uncertain inputs from that arising from the model's inherent stochasticity. This requires more sophisticated statistical techniques or variance decomposition methods to ensure meaningful sensitivity assessment<sup>43</sup>.

A wide variety of methods exist for conducting sensitivity analysis, many of which have been developed specifically to address the practical challenges outlined above. These methods differ not only in their computational strategies but also in the type of sensitivity measure they employ, ranging from variance-based decomposition (e.g. Sobol' indices), to local gradient-based techniques (e.g. partial derivatives), to screening methods (e.g. elementary effects). Despite these differences, most sensitivity analysis approaches begin by characterizing the uncertainty associated with each model input, typically through the definition of input ranges or probability distributions. However, accurately defining these uncertainties can itself be challenging, particularly when relying on expert judgment or limited data. In such cases, various elicitation techniques are available to infer probability distributions from qualitative or subjective sources<sup>44</sup>.

## Global sensitivity analysis

The goal of the Global Sensitivity Analysis is to identify the most impactful parameters from a total set of  $N$  input parameters on the response of a given system or process. One

---

<sup>41</sup> Chastaing, G., Gamboa, F., and Prieur, C., "Generalized Hoeffding-Sobol Decomposition for Dependent Variables - Application to Sensitivity Analysis," *Electronic Journal of Statistics*, Vol. 6, 2012.

<sup>42</sup> Gamboa, F., Janon, A., Klein, T., and Lagnoux, A., "Sensitivity Analysis for Multidimensional and Functional Outputs," *Electronic Journal of Statistics*, Vol. 8, No. 1, 2014.

<sup>43</sup> Marrel, A., Iooss, B., Da Veiga, S., and Ribatet, M., "Global Sensitivity Analysis of Stochastic Computer Models with Joint Metamodels," *Statistics and Computing*, Vol. 22, No. 3, 2012, pp. 833–847.

<sup>44</sup> O'Hagan, A., Buck, C. E., Daneshkhah, A., Eiser, J. R., Garthwaite, P. H., Jenkinson, D. J., Oakley, J. E., and Rakow, T., "Uncertain Judgements: Eliciting Experts' Probabilities," Wiley, 2006.

of the most well-known methods to implement a Global Sensitivity Analysis is the Sobol's method<sup>45</sup>. According to the latter, each function  $Y = f(\mathbf{X})$  that is dependent on a set of a total of  $N_p$  parameters can be expanded into summands of different dimensions, as shown in the following equation:

$$Y = f(\mathbf{X}) = f_0 + \sum_{n=1}^{N_p} f_n(x_n) + \sum_{1 \leq n \leq n' \leq N_p} f_{n,n'}(x_n, x_{n'}) + \dots + f_{1,2,\dots,N_p}(x_1, \dots, x_{N_p})$$

where the first summand reflects the contribution of each respective parameter, while the second one considers the interaction between the input parameters. In a similar way, the total variance of the function can be expanded into summands of different variances related to each respective parameter as follows:

$$Var(Y) = \sum_{n=1}^{N_p} D_n + \sum_{1 \leq n \leq n' \leq N_p} D_{n,n'} + \dots + D_{1,2,\dots,N_p}$$

where  $D_n = Var[E(Y|X_n)]$  is the variance due to the effect of each respective parameter, while  $D_{n,n'} = Var[E(Y|X_n, X_{n'})] - D_n - D_{n'}$ , is the variance due to the effect of the interaction between parameters. Then the sensitivity indices are introduced, which quantify the relative effect of the variance for each parameter compared to the overall variance, shown in the following equation:

$$S_n = \frac{D_n}{Var(Y)}$$

$$S_{n,n'} = \frac{D_{n,n'}}{Var(Y)}$$

$$S_{1,2,\dots,N_p} = \frac{D_{1,2,\dots,N_p}}{Var(Y)}$$

The calculation of all these indices leads to the estimation of first-order and total-order sensitivity indices. The first-order index ( $S_n$ ) considers only the sole contribution of each parameter to the total variance without including the interactions between the parameters, while the total-order index also includes the interactions, as shown in the following equation:

$$S_{T_n} = S_n + \sum_{n < n'} S_{n,n'} + \sum_{n' \neq n, n'' \neq n, n' < n''} S_{n,n',n''}$$

---

<sup>45</sup> Sobol I. M. "Global Sensitivity Indices for Nonlinear Mathematical Models and Their Monte Carlo Estimates." *Mathematics and Computers in Simulation*, vol. 55, no. 1-3, 2001, pp. 271–80.

The estimation of first-order and total-order sensitivity indices for complex functions, is typically achieved by using Saltelli sampling<sup>46,47</sup>. According to the latter, for each function of  $D$  dimensions  $Y = f(\mathbf{X}) = f(x_1, x_2, \dots, x_d)$ , a sample  $\mathbf{X}$  is created, featuring  $K \times D$  dimensions.

$$\mathbf{X} = \begin{bmatrix} x_{11} & x_{12} & \cdots & x_{1d} \\ x_{21} & x_{22} & \cdots & x_{2d} \\ \vdots & \vdots & \ddots & \vdots \\ x_{k1} & x_{k2} & \cdots & x_{kd} \end{bmatrix}$$

The total number  $K$  rows are estimated as  $K = N(2D + 2) \times D$ , where  $D$  is the number of dimensions and  $N$  is a number, typically selected as  $N = 1024$ . For the given input sample, the output sample of the function  $Y$  is calculated using a simple Monte-Carlo method.

$$Y = \begin{bmatrix} y_1 \\ y_2 \\ \vdots \\ y_k \end{bmatrix}$$

The output sample features  $N \times 1$  dimensions. Then, four matrices  $A$ ,  $B$ ,  $AB$ ,  $BA$  are generated based on the output sample,  $A$ ,  $B$  featuring  $N \times 1$  dimensions, and  $AB$ ,  $BA$  featuring  $N \times D$  dimensions.

$$A = \begin{bmatrix} y_1 \\ y_{(2D+2)+1} \\ \vdots \\ \vdots \end{bmatrix} \quad B = \begin{bmatrix} y_{2D+2} \\ y_{2*(2D+2)} \\ \vdots \\ \vdots \end{bmatrix}$$

$$AB = \begin{bmatrix} y_2 & y_3 & \cdots & y_{D+1} \\ y_{(2D+2)+2} & y_{(2D+2)+3} & \cdots & y_{(2D+2)+(D+1)} \\ \vdots & \vdots & \ddots & \vdots \\ \vdots & \vdots & \cdots & \vdots \end{bmatrix}$$

$$BA = \begin{bmatrix} y_{D+2} & \cdots & y_{(2D+2)-1} \\ y_{(2D+2)+D+2} & \cdots & y_{2*(2D+2)-1} \\ \vdots & \ddots & \vdots \\ \vdots & \cdots & \vdots \end{bmatrix}$$

<sup>46</sup> Saltelli A. "Making Best Use of Model Evaluations to Compute Sensitivity Indices." *Computer Physics Communications*, vol. 145, no. 2, 2002, pp. 280–97.

<sup>47</sup> Saltelli A., Annoni P., Azzini I., Campolongo F., Ratto M., and Tarantola S. "Variance Based Sensitivity Analysis of Model Output. Design and Estimator for the Total Sensitivity Index." *Computer Physics Communications*, vol. 181, no. 2, 2010, pp. 259–70.

Finally, the first-order and total-order sensitivity indices are calculated based on the following equations:

$$S_j = \frac{B[(AB)_j - A]}{\text{Var}\left(\begin{bmatrix} A \\ B \end{bmatrix}\right)} \quad \forall j \in 1, 2, \dots, D$$

$$S_{Tj} = \frac{\frac{1}{2} [A - (AB)_j]^2}{\text{Var}\left(\begin{bmatrix} A \\ B \end{bmatrix}\right)} \quad \forall j \in 1, 2, \dots, D$$

### 3.5. Reliability methods

Reliability methods are a class of uncertainty quantification techniques that aim to estimate the probability of failure or the likelihood that a system will perform its intended function under specified conditions. These methods are particularly important in engineering design where safety and robustness are critical. Their aim is to compute the limit-state function. A limit-state function is a mathematical representation that defines the boundary between the safe and failure states of a system. It is typically denoted as  $g(X) = 0$  where  $X$  is the vector of uncertain input parameters (e.g., loads, material properties). The function  $g(X)$  is constructed such that:

- $g(X) > 0$ : the system is in a safe state.
- $g(X) = 0$ : the system is at the limit of failure (limit-state).
- $g(X) < 0$ : the system has failed

In reliability analysis, the goal is to compute the probability that  $g(X) < 0$ , which corresponds to the probability of failure. The failure domain is also a quantity of interest in the reliability analysis context. It is the set of all input values  $X$  for which the system is considered to have failed. It is defined mathematically using the limit-state function  $g(X)$  as the set  $\{X \mid g(X) < 0\}$ . The form of the limit-state function depends on the specific engineering application and performance criteria being considered.

Traditional reliability approaches include First-Order Reliability Method (FORM) and Second-Order Reliability Method (SORM), which approximate the limit-state function near the design point to estimate small failure probabilities<sup>48</sup>. More recently, sampling-

---

<sup>48</sup> Ditlevsen, O., Madsen, H. O., and Ditlevsen, O., "Structural Reliability Methods," Wiley, Chichester, 1999.

based methods such as Monte Carlo sampling and importance sampling have been widely adopted due to their robustness, though they can be computationally demanding. Subset simulation<sup>49</sup> has been developed to address rare event estimation more efficiently by decomposing the failure event into a sequence of more probable intermediate events. In parallel, surrogate-based reliability methods, such as those using Gaussian process<sup>50</sup> or support vector machines<sup>51</sup>, have emerged to reduce computational costs by approximating the performance function. The failure domain can be effectively estimated and bounded for systems affected by parametric uncertainty and governed by multiple design constraints<sup>52,53</sup>, enabling a more accurate and efficient assessment of system reliability under complex performance requirements. These techniques are increasingly applied in aerospace, automotive, and structural engineering domains where reliability under uncertainty is paramount.

### 3.6. Application and software considerations

This project aims to harness the latest advancements in machine learning to create novel uncertainty quantification methods that tackle challenges such as the curse of dimensionality and the non-linear physics inherent in some engineering problems. Python has become the language of choice for uncertainty quantification due to its flexibility, ease of integration with other scientific computing tools, and its growing prominence in the machine learning field. In this project, we will use the open-source library PyTorch to develop advanced deep learning architectures<sup>54</sup>. PyTorch is widely adopted for its flexibility, ease of use, and strong support for both research and production environments. Several other open-source Python libraries have been developed to support uncertainty quantification methods, each offering a range of tools for various applications. OpenTURNS<sup>55</sup> (Open-source Treatment of Uncertainty, Risk 'N Statistics) is a comprehensive library for probabilistic modelling and UQ, supporting techniques like Monte Carlo simulations, sensitivity analysis, and surrogate modelling.

---

<sup>49</sup> Au, S.-K., and Beck, J. L., "Estimation of Small Failure Probabilities in High Dimensions by Subset Simulation," *Probabilistic Engineering Mechanics*, Vol. 16, No. 4, 2001, pp. 263–277.

<sup>50</sup> Echard, B., Gayton, N., and Lemaire, M., "AK-MCS: An Active Learning Reliability Method Combining Kriging and Monte Carlo Simulation," *Structural Safety*, Vol. 33, No. 2, 2011, pp. 145–154.

<sup>51</sup> Pepper, N., Crespo, L., and Montomoli, F., "Adaptive Learning for Reliability Analysis Using Support Vector Machines," *Reliability Engineering & System Safety*, Vol. 226, 2022, p. 108635.

<sup>52</sup> Crespo, L. G., Giesy, D. P., and Kenny, S. P., "Reliability-Based Analysis and Design via Failure Domain Bounding," *Structural Safety*, Vol. 31, No. 4, 2009, pp. 306–315.

<sup>53</sup> Crespo, L. G., Kenny, S. P., and Giesy, D. P., "Reliability Analysis of Polynomial Systems Subject to P-Box Uncertainties," *Mechanical Systems and Signal Processing*, Vol. 37, Nos. 1–2, 2013, pp. 121–136.

<sup>54</sup> Imambi, Sagar, Kolla Bhanu Prakash, and G. R. Kanagachidambaresan. "PyTorch." *Programming with TensorFlow: Solution for Edge Computing Applications*, 2021, pp. 87–104. <https://pytorch.org/>

<sup>55</sup> Baudin, M., A. Dutfoy, B. Iooss, and A. L. Popelin. "OpenTURNS: An Industrial Software for Uncertainty Quantification in Simulation." *Handbook of Uncertainty Quantification*, Springer, Cham, 2017, pp. 2001–2038. <https://openturns.github.io/www/>

Chaospy<sup>56</sup> is a Python library focused on polynomial chaos expansions and sampling techniques, which is particularly useful for applications requiring stochastic models.

Concerning the implementation of Global Sensitivity Analysis using the Sobol's method, SALib<sup>57</sup> is one of the most acknowledged open-access libraries that enables the integration of these methods in a Python environment in an easy and standardized way. The implementation of SALib can be summarized in four main steps: i) determining input parameters and sample range, ii) executing the given function for the input sample, iii) generating and evaluating the resulting output sample, and iv) analyzing the results, generating the respective matrices, and calculating the sensitivity indices.

---

<sup>56</sup> Feinberg, Jonathan, and Hans Petter Langtangen. "Chaospy: An Open Source Tool for Designing Methods of Uncertainty Quantification." *Journal of Computational Science*, vol. 11, 2015, pp. 46–57. <https://chaospy.readthedocs.io/en/master/>

<sup>57</sup> Iwanaga, T., W. Usher, and J. Herman. "Toward SALib 2.0: Advancing the Accessibility and Interpretability of Global Sensitivity Analyses." *Socio-Environmental Systems Modelling*, vol. 4, 2022, p. 18155.

## 4. Preliminary characterisation in H<sub>2</sub>-powered propulsion components

The characterisation and quantification of the wide range of uncertainties that arise throughout a complex system's life cycle remain largely unexplored, particularly in understanding how these uncertainties propagate across various subsystems. This project aims to address two key objectives: first, to characterize uncertainties based on the fidelity level of each system; and second, to assess uncertainties at different stages of the system life cycle. While much of the existing literature concentrates on conventional fuel-powered aircraft, the uncertainty characterisation undertaken in this work must be tailored to the unique technological and operational aspects of hydrogen-powered aircraft.

### 4.1. Design and development

#### 4.1.1. Uncertainties in aircraft engine design

The characterization of uncertainties related to aero engine performance is important when aiming for a robust engine design. Hence, this section aims to introduce the various sources of uncertainty revolving around aero engine performance. In addition, it proposes a flow of calculations to quantify the effect of all uncertainties on the engine design. The section starts with compartmentalizing the uncertainties based on their source (Manufacturing deviations, component design and Growth potential) along with the variations proposed by literature on every respective source. Then, the final subsection begins by reviewing the way uncertainty quantification is implemented in various cases and concludes with the proposed methodology that will be employed in this project for uncertainty quantification on aero engine performance.

## Effect of manufacturing tolerances

Gas turbine manufacturing processes, even in well controlled environments, introduce small geometrical deviations between individual compressors, turbines, ducts, and nozzles. These deviations translate to significant engine to engine performance variations and even though the engine designers study the average engine produced by the assembly line, a guarantee must be given that the required performance level will be achieved even for the (worst case) minimum engine<sup>58,59</sup>. In addition, as the engine core size decreases, manufacturing uncertainties have a greater impact on its performance<sup>60</sup>.

While tolerances are less significant for fans, compressors are highly affected by small variations, mainly due to the adverse pressure gradient on the airfoils. Small errors in the front stages propagate and amplify downstream. Four areas have been identified as the most influential for compressor performance: (i) Leading edge shape, (ii) rotor tip gap, (iii) airfoil roughness, and (iv) real geometry features such as fillets, leakages, and inter-platform gaps.

- (i) Leading edges in axial compressors have a radius of around 0.1 mm. The response of a compressor to geometrical variations is nonlinear. Small variations in the leading edge can thicken the boundary layer on the early suction side and increase the size of three-dimensional separations. When these variations are considered, a reduction of 1.2% in efficiency can be observed in the case of a six-stage compressor. Erosion does not seem to significantly affect the performance of high-pressure compressors, and they are mainly dominated by manufacturing errors.
- (ii) For tip gaps from 0.5 to 0.8%, a gap decrease reduces the tip leakage mixing losses while it increases viscous shear losses. For gaps between 0.8 and 3.4%, efficiency decreases by 1 point for every 1% increase in tip gap.
- (iii) Regarding airfoil roughness, the leading edge and front half of the suction side are the most critical regions.
- (iv) Real geometry effect is a very broad term, but regarding fillets, the larger it is, the greater the loss.

Furthermore, manufacturing tolerances also affect High-Pressure Turbines (HPTs), as the latter are highly loaded and subject to strong thermal gradients. Therefore, small variations can greatly affect the engine reliability. While for compressors, these

---

<sup>58</sup> Kurzke, J., and I. Halliwell. *Propulsion and Power: An Exploration of Gas Turbine Performance Modeling*. Springer, 2018.

<sup>59</sup> Walsh, P., and P. Fletcher. *Gas Turbine Performance*. John Wiley & Sons, 2004.

<sup>60</sup> Montomoli, F., M. Carnevale, A. D'Ammaro, M. Massini, and S. Salvadori. *Uncertainty Quantification in Computational Fluid Dynamics and Aircraft Engines*. Springer International Publishing, 2015, pp. 1–90.

variations affect mainly efficiency, in the case of turbines, the main concern is the lifetime of the hot components. In the case of Low-Pressure Turbines (LPTs), the effect of blade roughness does not have a significant effect on LPT efficiency, nor does the trailing edge thickness or the airfoil thickness in general. To account for the manufacturing tolerances Kurzke<sup>58,61</sup> proposed the following uncertainties for the engine key parameters which are summarized in

Table 1.

**Table 1.** Characterization of engine design uncertainties related to manufacturing deviations, according to existing literature

Parameter	Units	Type	Standard Deviation	Nature of Uncertainty	Ref.
Low Pressure compressor Corrected Mass Flow (Axial)	(rel., %)	Aleatoric	± 0.25 %	Manufacturing Tolerances	[58,61]
High Pressure compressor Corrected Mass Flow (Cf.)	(rel., %)	Aleatoric	± 0.25 %	Manufacturing Tolerances	[58,61]
Low Pressure compressor efficiency (Axial)	(rel., %)	Aleatoric	± 0.25%	Manufacturing Tolerances	[58,61]
High Pressure compressor efficiency (Cf.)	(rel., %)	Aleatoric	± 0.25%	Manufacturing Tolerances	[58,61]
High Pressure Turbine Corrected Mass Flow	(rel., %)	Aleatoric	± 0.3%	Manufacturing Tolerances	[58,61]
Low Pressure Turbine Corrected Mass Flow	(rel., %)	Aleatoric	± 0.1%	Manufacturing Tolerances	[58,61]
High Pressure Turbine efficiency	(rel., %)	Aleatoric	± 0.3%	Manufacturing Tolerances	[58,61]
Low Pressure Turbine efficiency	(rel., %)	Aleatoric	± 0.2%	Manufacturing Tolerances	[58,61]

## Uncertainties during engine design phase

During the development phase, when the main requirements of the engine are determined and the different components are sized, designers typically work with the “most likely” component efficiencies estimated by the component specialists. However, the actual component efficiencies after the engine assembly can introduce non-negligible variations compared to the initial design assumptions. Uncertainties introduced due to these deviations can either be depicted through TET or engine power and if they are not taken into consideration, engine power requirements and safety will possible not meet the design requirements. Walsh and Flecher<sup>59</sup> estimated that,

<sup>61</sup> Kurzke, J. “Some Applications of the Monte Carlo Method to Gas Turbine Performance Simulations.” *Proceedings of the ASME 1997 International Gas Turbine and Aeroengine Congress and Exhibition*, vol. 4, ASME, 1997, Paper No. V004T16A003, Orlando, Florida, 2–5 June 1997.

depending on the components specialists estimations confidence, a design power margin between +2.5% and +7.5% should be considered. A drawback of this approach is that these margins may be overestimated, leading to unnecessary performance deterioration<sup>62</sup>.

Regarding the component design uncertainties Kurzke and Halliwell<sup>58</sup> propose that after discussing with the component specialists, their most optimistic, most likely and most pessimistic guesses for components efficiency should be recorded. Then, the triangular distribution for component efficiency is defined by the triangle whose two corners correspond to the most optimistic and most pessimistic guesses respectively, while the third corner corresponds to the most likely guess. The proposed efficiency uncertainties are summarized in Table 2.

**Table 2.** Characterization of engine design uncertainties due to engine-to-engine scatter, according to existing literature

Parameter	Units	Type	Range			Nature of Uncertainty	Ref.
			Min	Mode	Max		
Low Pressure Turbine Corrected Mass Flow	(rel., %)	Aleatoric	-2.0%	0.0%	+0.5%	Component design shortfall	[58,59]
High Pressure Turbine efficiency	(rel., %)	Aleatoric	-2.0%	0.0%	+0.5%	Component design shortfall	[58,59]
Low Pressure Turbine efficiency	(rel., %)	Aleatoric	-2.0%	0.0%	+0.5%	Component design shortfall	[58,59]

### Uncertainties during aircraft design and due to potential engine growth

Engine power or thrust requirements are originating from the demands of the aircraft designer which change through the course of the respective design process and most of the times, increase. Additionally, engines usually become economically more attractive when they are capable of adapting to higher power or thrust levels, since the same development cost can lead to a technology covering a wider market range. These uncertainty factors should be accounted for by incorporating a design power margin.

### Uncertainties treatment in aircraft engine performance - Literature

This subsection begins with a literature review on works related with the treatment of uncertainties in aircraft engine performance related topics and then continues with the introduction of the uncertainty quantification implementation of this project. Although limited, several studies in existing literature have focused on the uncertainty quantification regarding the performance and reliability of gas turbines and aircraft

<sup>62</sup> Csavina, F. L., and Russell K. D. "A Global Approach in Evaluating Inlet/Engine Compatibility." *Turbo Expo: Power for Land, Sea, and Air*. Vol. 78996. American Society of Mechanical Engineers, 1991.

engines specifically. The majority of studies in existing literature dealing with the uncertainty impact during the engine performance modelling phase employ the Monte Carlo method<sup>58,61,63,64,65</sup>. The latter requires the use of predefined statistical distributions to simulate the uncertainty of each parameter.

Considering aero-engine performance modelling, Liu et al.<sup>66</sup> developed an uncertainty quantification (UQ) method for a turboshaft aero-engine by combining statistical sampling with a surrogate model. Traditional Monte Carlo design of experiment creation is accurate but computationally expensive. To overcome this issue, a method is proposed that maintains accuracy while reducing the computational cost. In more detail, the objective was to assess how a variability in six component performance parameters (flow capacity and adiabatic efficiency of compressor, HPT, LPT) affects engine performance. Each parameter was modelled as a truncated Gaussian ( $\pm 0.02$  around nominal, covering  $\sim 99.7\%$  range). The methodology included the creation of a Latin Hypercube Sampling (LHS) design with a sample of 1,000 points. Then three Gaussian Process surrogates were trained to predict engine outputs: output power ( $P_e$ ), specific fuel consumption (SFC), and HPT outlet temperature ( $T_{45}$ ). The LHS was used together with the trained surrogates to propagate uncertainties (with  $n=20,000 + 100$  replicates) and estimate means, standard deviations, and sensitivity indices.

Some of the key quantitative results were the effect of component standard deviations ( $\sigma_{input} = 0.002$  to  $0.004$ ). By assuming 60% correlation between compressor flow and efficiency the output power standard deviation decreases by 6.6-8.7% versus the independent case. The  $T_{45}$  decreases by 2.3-4.2% and SFC increases slightly by 3.0-3.7%. Regarding the uncertainty magnitudes reported, while the exact output baseline was confidential, reported relative uncertainties (assuming  $\sigma_{input} = 0.003$ ) were approximately:  $\sigma_{pe} = 2 - 3\%$  of nominal,  $\sigma_{SFC} = 1 - 2\%$ ,  $\sigma_{T45} = 1 - 1.5\%$ .

The Gaussian Process Model (GPM)-LHS was compared with a simulation-based Monte Carlo and showed excellent fidelity, with the prediction error being smaller than the sampling uncertainty. The combination of  $n=20,000$  LHS runs with 100 replicates allowed estimation of total uncertainty contributions (approximation + sampling). Convergence was achieved much faster than brute-force Monte Carlo (e.g.,  $10^5$

<sup>63</sup> Abernethy, R., and J. Sammons. "Three Applications of Monte Carlo Simulation to the Development of the F100 Turbofan Engine." *Proceedings of the 12th Propulsion Conference*, 1976, p. 731

<sup>64</sup> Zhang, J., H. Tang, and M. Chen. "Robust Design of an Adaptive Cycle Engine Performance under Component Performance Uncertainty." *Aerospace Science and Technology*, vol. 113, 2021, p. 106704.

<sup>65</sup> Youngmans, J. L., J. E. Johnson, and S. J. Csonka. "A Methodology to Assess Design Uncertainty in Selecting Affordable Gas Turbine Technology." *Journal of Engineering for Gas Turbines and Power*, vol. 117, no. 4, Oct. 1995, pp. 666–672.

<sup>66</sup> Liu, X., H. Tang, X. Zhang, and M. Chen. "Gaussian Process Model-Based Performance Uncertainty Quantification of a Typical Turboshaft Engine." *Applied Sciences*, vol. 11, no. 18, 2021, p. 8333.

samples), offering  $\sim 100\times$  computational speed-up. Furthermore, a sensitivity analysis based on Sobol first-order indices showed that Compressor efficiency ( $\eta_C$ ) was a dominant factor, contributing  $\sim 40\text{-}50\%$  of variance in both  $P_e$  and SFC. On the other hand, Turbine efficiency ( $\eta_T$ ) was a major contributor to  $T_{45}$  variability. Other parameters like flow capacities and LPT variables had lesser influence ( $\sim 10\text{-}20\%$ ).

Furthermore, in another study, Cajahuaringa et al.<sup>67</sup> developed a hybrid data-driven model for a Gas Turbine (GT) aiming to estimate the rotational speed. In more detail, a Siemens SGT6-5000F gas turbine with 215 MW power output was studied. The inputs for the models were fuel flow, inlet air temperature, and barometric pressure. Three models were used for simulation: a nonlinear autoregressive with exogenous input recurrent neural network (NARX-RNN), an NARX-LSTM, and a pure LSTM. These models estimated the RPM of the gas turbine. The metrics used for the analysis and evaluation of the model were the mean square error (MSE), mean average error (MAE), and mean average percentage error (MAPE). On the table, the comparison of the architectures is presented.

**Table 3.** Evaluation metrics in the rotation speed estimation<sup>67</sup>.

Model	NARX-RNN	NARX + LSTM	LSTM
MSE	1.8	5.22	7.62
MAE	0.98	1.78	2.15
MAPE	0.02%	0.045%	0.055%
Training Time (s)	41.88	85.09	121.32

The NARX-RNN model outperformed the others, with the lowest error and fastest training. To quantify the uncertainty Monte Carlo Dropout was used. Wenqiang et al.<sup>68</sup>, tried to evaluate how uncertainties in key gas turbine component parameters propagate to system-level performance (output power, efficiency, exhaust temperature). The model created was one of an aero-derivative gas turbine using thermal-process equations. The uncertain inputs in this study, used as independent or coupled, were the compressor efficiency ( $\eta_p$ ), compressor inlet flow ( $\dot{m}_a$ ), turbine efficiency ( $\eta_t$ ), and cooling air flow ( $\dot{m}_{cool}$ ). The methodology developed in this study consisted of Monte Carlo (MC) simulations that executed thousands of samples. Two scenarios were analyzed. One where the uncertainties were independent, meaning that each parameter varied separately. The second scenario included coupled uncertainties where there was simultaneous variation of parameters. The distributions for each parameter, Gaussian or uniform, were sampled to propagate through the model. The turbine efficiency exhibited the largest impact across all performance outputs. The compressor efficiency had a

<sup>67</sup> Cajahuaringa, A., R. A. Palacios, J. M. Mauricio Villanueva, A. Morales-Villanueva, J. Machuca, J. Contreras, and K. Rodríguez Bautista. "Uncertainty Evaluation of a Gas Turbine Model Based on a Nonlinear Autoregressive Exogenous Model and Monte Carlo Dropout." *Sensors*, vol. 24, no. 2, 2024, p. 465.

<sup>68</sup> Wenqiang, L., Yan, C., Jinglun, F., Haisong, L., and Xiangling, K. "Uncertainty Analysis of Gas Turbine Overall Performance Based on Monte Carlo Method." *Power Generation Technology*, vol. 46, no. 1, 2025, p. 126.

strong influence too, but its impact was diminishing when multiple uncertainties were combined. Most importantly, the variability in the output power peaked when turbine efficiency uncertainty was included, while other parameters had lesser effect.

The main outcomes from the examined studies in existing literature, regarding the uncertainty quantification methods used, the application, as well as the respective strengths and limitations are summarized in the following table (Table 4).

**Table 4.** Summary of key outcomes of selected studies in existing literature, regarding the uncertainty quantification of gas turbines and aircraft engines.

Application	Uncertainty Method	Methodology Strengths	Specific scope and assumptions	Ref.
Performance prediction under component variability (flow, efficiency)	Gaussian Process surrogate + Latin Hypercube Sampling (LHS); Sobol sensitivity indices	<ul style="list-style-type: none"> <li>• Accurate surrogate models</li> <li>• Efficient sampling (fast vs MC)</li> <li>• Includes correlation effects</li> </ul>	<ul style="list-style-type: none"> <li>• No absolute output values</li> <li>• Limited to <math>\pm 2\%</math> parametric variations</li> <li>• Based on static performance model</li> </ul>	[66]
Predictive modeling of shaft speed using ML with UQ	Monte Carlo Dropout on NARX-RNN and LSTM architectures	<ul style="list-style-type: none"> <li>• Combines ML accuracy and uncertainty</li> <li>• Fast &amp; low-resource</li> <li>• Standard deviation <math>\sim 2.2</math> RPM</li> </ul>	<ul style="list-style-type: none"> <li>• Focused on RPM only</li> <li>• Only epistemic uncertainty captured</li> <li>• - Manual architecture tuning</li> </ul>	[67]
Overall gas turbine performance (output power, efficiency, exhaust temp.) under component uncertainty	Classic Monte Carlo with independently coupled uncertain inputs	<ul style="list-style-type: none"> <li>• Highlights dominant role of turbine efficiency</li> <li>• Broad system-level insight</li> <li>• Considers coupled vs. uncoupled cases</li> </ul>	<ul style="list-style-type: none"> <li>• No quantitative outputs (e.g., <math>\sigma</math>)</li> <li>• Lacks sensitivity metrics</li> <li>• Unclear distributions/sample size</li> </ul>	[68]

## DEMOQUAS proposed implementation

After the introduction of the different approaches found in literature, uncertainty quantification is proposed to be treated with a TET stack up at the thermally most challenging phase, the reserve take-off hot-day conditions. In more detail, take-off

design TET value is estimated for most-likely component design efficiencies. This sized engine is evaluated against all the possible uncertainty cases, by type, at off-design conditions, without imposing any thermal constraints to the engine. More specifically, manufacturing uncertainties are first treated to quantify the TET increase required to cover the minimum engine. Then a separate analysis is performed, considering the uncertainties introduced by a potential component efficiency shortfall relative to the values used for design, again, to calculate how much the TET should increase to satisfy the guaranteed power. Finally, the engine growth potential and oversizing due to aircraft requirements are studied to quantify the additional TET required from this source. Finally, these three increasing factors of the TET are added and give the margin that needs to be considered (engine cycle design maximum TET) relative to the maximum TET value allowed by the materials (redline TET).

Considering various literature sources, a prediction for the stack up contributions from the three main engine uncertainties is proposed in Table 5. In addition, there is a final contribution to the TET stack up by the engine degradation calculations as even a fully deteriorated engine has to still satisfy the guaranteed power. This factor is not related to performance uncertainties but rather the natural components degradation over time. Such a first estimation is offered here<sup>69</sup>, presented in Table 5 .

**Table 5.** Turbine Entry Temperature margin stack-up due to various sources of uncertainty according to literature.

Sources of potential TET increase	Margin	Ref.
Component design shortfall	To be determined	
Manufacturing tolerances	+ 20 K	[59]
Growth Potential	To be determined	
Engine degradation	+ 30 K	[69]

No clear suggestion was found in the literature as to how to introduce the manufacturing uncertainties and thus it is assumed that their variation follows a Gaussian normal distribution with mean equal to the baseline value and standard deviations equal to those of

Table 1. Compressor efficiency is correlated with flow capacity (mass flow), which in turn correlates to the component pressure ratio. When efficiency changes, due to manufacturing tolerances, a following change of mass flow occurs and hence, a change in pressure ratio should also be considered for since the engine remains on the same speed line.

<sup>69</sup> Pratt & Whitney, "Pratt & Whitney Canada Maintenance Manual No.3045542", 2006

Regarding the component design shortfall uncertainties, the triangular distributions proposed by Kurzke and Halliwell<sup>58</sup> will be integrated, which is consistent with the approaches used in other studies<sup>65</sup>. To summarize on the introduced uncertainties and their treatment Table 6 depicts all the required information for the uncertainty quantification per uncertainty source.

**Table 6.** Summary of proposed preliminary characterization of engine performance uncertainties.

Component design shortfall								
Parameter	Units	Type	Distribution	Range			Nature of Uncertainty	Ref.
				Min.	Mode	Max.		
High Pressure compressor efficiency (Cf.)	(rel., %)	Aleatoric	Triangular	-2.0%	0.0%	+0.5%	Component design shortfall	[58,61]
High Pressure Turbine efficiency	(rel., %)	Aleatoric	Triangular	-2.0%	0.0%	+0.5%	Component design shortfall	[58,61]
Low Pressure Turbine efficiency	(rel., %)	Aleatoric	Triangular	-2.0%	0.0%	+0.5%	Component design shortfall	[58,61]
Manufacturing								
Parameter	Units	Type	Distribution	Std. Dev. ( $\sigma$ )	Nature of Uncertainty		Ref.	
					Tolerances			
Low Pressure compressor Corrected Mass Flow (Axial)	(rel., %)	Aleatoric	Gaussian	$\pm 0.25\%$	Manufacturing Tolerances		[58,59]	
High Pressure compressor Corrected Mass Flow (Cf.)	(rel., %)	Aleatoric	Gaussian	$\pm 0.25\%$	Manufacturing Tolerances		[58,59]	
Low Pressure compressor efficiency (Axial)	(rel., %)	Aleatoric	Gaussian	$\pm 0.25\%$	Manufacturing Tolerances		[58,59]	
High Pressure compressor efficiency (Cf.)	(rel., %)	Aleatoric	Gaussian	$\pm 0.25\%$	Manufacturing Tolerances		[58,59]	
High Pressure Turbine Corrected Mass Flow	(rel., %)	Aleatoric	Gaussian	$\pm 0.3\%$	Manufacturing Tolerances		[58,59]	
Low Pressure Turbine Corrected Mass Flow	(rel., %)	Aleatoric	Gaussian	$\pm 0.1\%$	Manufacturing Tolerances		[58,59]	
High Pressure Turbine efficiency	(rel., %)	Aleatoric	Gaussian	$\pm 0.3\%$	Manufacturing Tolerances		[58,59]	
Low Pressure Turbine efficiency	(rel., %)	Aleatoric	Gaussian	$\pm 0.2\%$	Manufacturing Tolerances		[58,59]	
Environmental control system Bleed Mass Flow Rate	(abs., kg/s)	Aleatoric	Gaussian	$\pm 0.1$	Manufacturing Tolerances		[58,59]	

#### 4.1.2. Uncertainties in thermal management systems

##### Description of Thermal Management System architecture

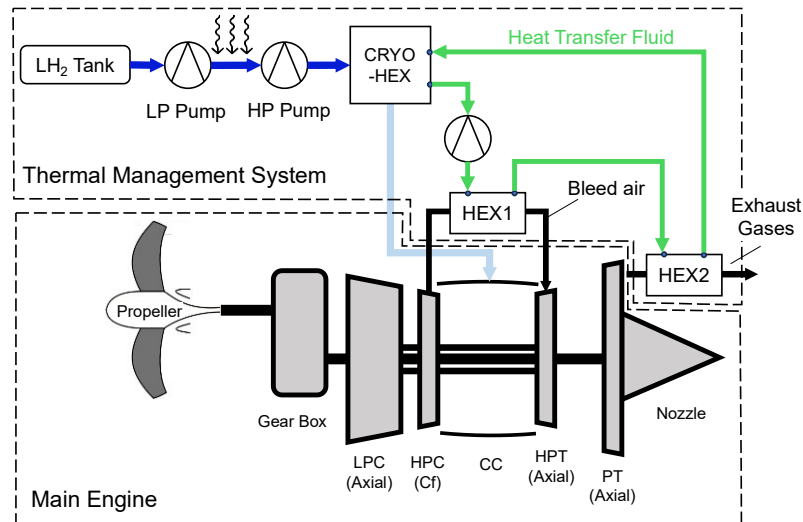


**Figure 5.** Thermal Management System architecture considered for the investigation.

When developing the H<sub>2</sub>-power engine, a fundamental difference compared to the baseline kerosene engine is the integration of the thermal management system (TMS), which is responsible for the preheating of the H<sub>2</sub> fuel, utilizing various heat sources from the main engine. A typical architecture of a thermal management system is shown in Figure 5. The system consists of a fuel circuit with a secondary cycle for fuel heating and 2 cryogenic pumps. The two-stage compression process is selected to avoid hydrogen evaporation in the pipes. The secondary cycle consists of a closed cycle featuring multiple heat exchangers, connecting the cryogenic fuel with the heat sources with an additional loop of an inert heat transfer fluid. The heat transfer fluid can be various gaseous or liquid mediums (i.e. helium, nitrogen, etc.).

As the TMS is connected with the aircraft engine, it is significantly affected by the uncertainties of the engine performance. Furthermore, additional uncertainties can further accumulate to the existing ones that are related mainly to the heat exchanger components.

##### Uncertainty treatment in heat exchanger design: Effect of manufacturing tolerances

State-of-the-art heat exchanger designs exhibit significantly small dimensions to increase compactness, hence manufacturing uncertainties are significant, as they are comparable to the design values. Moreover, small dimensions are prone to severe

fouling and blockage, further increasing the uncertainty of the flow field. Abdelaziz and Radermacher<sup>70</sup> tried to quantify these uncertainties for an air-to-water heat exchanger, by using the Monte Carlo simulation approach and CFD simulation. The uncertain parameters considered were the heat exchanger vertical spacing, and the water flow rate with a predefined normal (Gaussian) distribution, with maximum variability set at  $\pm 2\sigma$ . The results showed that enlarging the diameter increases the impact of geometric variability, while reducing the diameter increases the impact of flow rate variability.

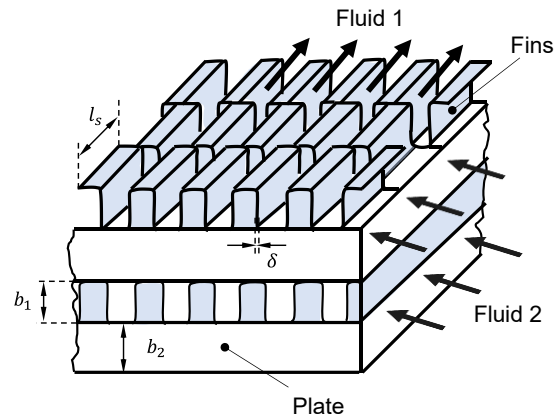


**Figure 6.** Typical offset strip plate-fin heat exchanger geometry considered for the Thermal Management System.

The heat exchanger components in such aerospace applications typically consist of compact geometries, such as offset strip fin-plate geometries<sup>77</sup>. (Figure 6) These geometries are typically manufactured using additive manufacturing techniques<sup>71,72</sup>, especially for hydrogen applications, where welded geometries are forbidden to avoid permeation. During the manufacturing process, there is always a deviation compared to the design dimensions, which must be below a maximum specified tolerance. London<sup>73</sup> proposed a manufacturing tolerance for the fin dimensions around  $\pm 10\%$  of their nominal values. Assuming the use of more advanced and state-of-the-art manufacturing techniques these tolerances can be further reduced, given also the high requirements for the aerospace applications studied here. One common additive manufacturing technique for these applications is direct metal laser sintering (DMLS)<sup>71,74</sup>. The method is expected to achieve a minimum tolerance around  $\pm 0.2$  mm (or  $\pm 0.2\%$  for small dimensions)<sup>75</sup>.

<sup>70</sup> Abdelaziz, O., and R. Radermacher. "Modeling Heat Exchangers under Consideration of Manufacturing Tolerances and Uncertain Flow Distribution." *International Journal of Refrigeration*, vol. 33, no. 4, 2010, pp. 815–828.

<sup>71</sup> Niknam, S. A., M. Mortazavi, and D. Li. "Additively Manufactured Heat Exchangers: A Review on Opportunities and Challenges." *The International Journal of Advanced Manufacturing Technology*, vol. 112, no. 3, 2021, pp. 601–618.

<sup>72</sup> *Heat Exchangers | Aerospace*. 3D Systems, <https://www.3dsystems.com/aerospace-defense/heat-exchangers>. Accessed 13 June 2025.

<sup>73</sup> London, A. L. "Laminar Flow Gas Turbine Regenerators—The Influence of Manufacturing Tolerances." *Journal of Engineering for Power*, vol. 92, no. 1, Jan. 1970, pp. 46–56

<sup>74</sup> Kaur, I., and P. Singh. "State-of-the-Art in Heat Exchanger Additive Manufacturing." *International Journal of Heat and Mass Transfer*, vol. 178, 2021, p. 121600.

<sup>75</sup> *Tolerances & Accuracy in 3D Printing Technologies*. Xometry, 15 Apr. 2025, <https://xometry.pro/en-eu/articles/3d-printing-tolerances/>. Accessed 27 June 2025.

During the design phase, a maximum tolerance is given by the designer (i.e.,  $\pm 0.2$  mm). Probabilistic uncertainty information is yet unknown in this stage, as no other information is required other than the variability bounds of each parameter in order to identify the “worst-case” scenario. The design tolerances concern mainly the heat exchanger fin dimensions (i.e. plate spacing, fin length, plate thickness etc.), which can be accounted for with tolerances in the hydraulic diameter ( $D_h$ ), the heat transfer areas, the fin-to-total area ratio ( $A_f/A$ ) and the total heat transfer area-to-volume ratio ( $\beta$ ) for each given geometry. The overall aim during the heat exchanger design is to determine the deviations in the overall weight and volume between the actual manufactured component and original design.

To quantify the effect of the heat exchanger fin tolerances on the hydraulic diameter, fin-to-total area ratio and the total heat transfer area-to-volume ratio, a preliminary Monte Carlo method was employed. Specifically, a set of 408 different TMS heat exchangers was examined, featuring various dimensions corresponding to effectiveness values from 0.08 up to 0.90. The methodology to calculate these parameters is presented in the Annex and is based on the methodology proposed by Shah and Sekulic<sup>76</sup>. As uncertainties are considered non-probabilistic at this phase, a uniform distribution is assumed for all parameters. According to the respective dataset, it was estimated that given the same tolerance for the plate-fin dimensions ( $\pm 0.2$  mm) the overall uncertainty in the investigated parameters is found in the range between -5.0% to 5.0%, which are shown in Figure 7. Taking everything into consideration, the proposed final tolerances that should be included in the design phase of the heat exchangers for the TMS are summarized in Table 7.

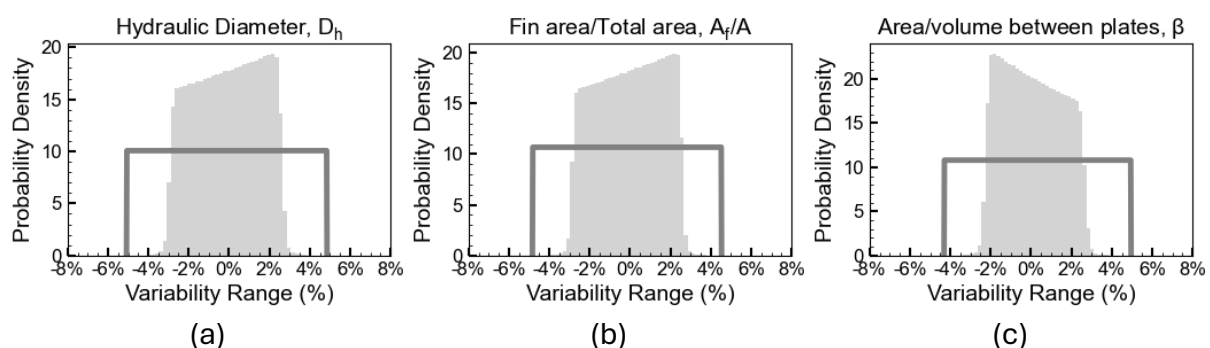


**Figure 7.** Maximum uncertainty range for the hydraulic diameter (a), the fin-to-total area ratio (b) and the total heat transfer area-to-volume ratio (c) estimated for the selected dataset of heat exchangers, based on the respective design tolerances.

<sup>76</sup> Shah, R. K., and D. P. Sekulic. *Fundamentals of Heat Exchanger Design*. John Wiley & Sons, 2003.

**Table 7.** Selected tolerances for the heat exchanger dimensions in the design phase.

Parameter	Units	Type	Distribution	Range		Nature of Uncertainty	Ref.
				Min.	Max.		
Plate spacing ( $b_i$ )	(abs., mm)	Epistemic	Uniform	-0.2	+0.2	Design Tolerances	[75]
Fin offset length ( $l_s$ )	(abs., mm)	Epistemic	Uniform	-0.2	+0.2		[75]
Fin metal thickness ( $\delta$ )	(rel., %)	Epistemic	Uniform	-0.2%	+0.2%		[75]
Plate thickness ( $\delta_w$ )	(rel., %)	Epistemic	Uniform	-0.2%	+0.2%		[75]
Hydraulic Diameter ( $D_h$ )	(rel., %)	Epistemic	Uniform	-5.0%	+5.0%		[76]
Fin area-to-Total area ratio ( $A_f/A$ )	(rel., %)	Epistemic	Uniform	-5.0%	+5.0%		[76]
Total heat transfer area-to-volume ratio between plates ( $\beta$ )	(rel., %)	Epistemic	Uniform	-5.0%	+5.0%		[76]

### Uncertainty treatment in heat exchangers: Uncertainties of non-dimensional numbers

One of the most common sources of uncertainty in heat exchangers is the uncertainty of the heat transfer coefficients. These coefficients are calculated based on non-dimensional numbers like the Reynolds and the Nusselt numbers, which are typically provided by experimental data. Therefore, these data are expected to exhibit measurement uncertainties. Kays and London<sup>77</sup> provided various experimental data of these non-dimensional numbers for various compact heat exchanger geometries. The main sources of uncertainty that they identified for the measured data were uncertainties inherent in the design and performance of the test system and instrument uncertainty. Based on this, they proposed some conservative estimations about the uncertainty range of key heat exchanger performance parameters. For the purpose of uncertainty treatment in the heat exchanger modelling, it is proposed to assume Gaussian distributions, where the proposed range corresponds to a confidence of  $\pm 2\sigma$ , in order to encompass 95.5% of the total distribution. The proposed uncertainties are summarized in the following table. Given the latter, a Monte Carlo method can be used to quantify the resulting uncertainty of the heat exchanger performance (i.e. hydrogen outlet temperature).

**Table 8.** Summary of key uncertainties in the non-dimensional numbers for various compact heat exchanger geometries reported by Kays and London.

Parameter	Units	Type	Distribution	St. Dev. ( $\sigma$ )	Nature of Uncertainty	Ref.
Colburn factor / Nusselt number ( $j$ ) / ( $Nu$ )	(rel., %)	Aleatoric	Gaussian	$\pm 2.5$ %	Experimental Uncertainty	[77]
Friction factor ( $f$ )	(rel., %)	Aleatoric	Gaussian	$\pm 2.5$ %	Experimental Uncertainty	[77]
Reynolds number ( $Re$ )	(rel., %)	Aleatoric	Gaussian	$\pm 1$ %	Experimental Uncertainty	[77]
Prandtl number ( $Pr$ )	(rel., %)	Aleatoric	Gaussian	$\pm 2.5$ %	Experimental Uncertainty	[77]

<sup>77</sup> Kays, W. M., and A. L. London. *Compact Heat Exchangers*. 3rd ed., McGraw-Hill, 1984.

## Uncertainty treatment in heat exchangers: Thermophysical properties

The determination of the heat transfer coefficients is affected by thermophysical properties, which are typically estimated through empirical correlations based on experimental data and yield a non-negligible uncertainty. Clarke et al.<sup>78</sup> investigated the effect of physical properties on the overall uncertainty of heat exchangers properties. Physical properties such as specific heat capacity ( $C_p$ ), density ( $\rho$ ), viscosity ( $\mu$ ), and thermal conductivity ( $k$ ) can exhibit uncertainties related to fitting accuracy (e.g., around 5%), especially for non-ambient conditions (e.g., high temperatures). Specifically at high temperatures, available experimental data are scarce, and physical properties estimation relies on extrapolation or predictive models. These models typically yield both systematic and random errors that can propagate and contribute to the overall uncertainty in heat exchanger design; however, systematic errors are typically neglected in existing literature. The proposed methodology attempted to define the true uncertainty in the heat exchanger design by providing a probabilistic evaluation for each variable of interest. This can facilitate the determination of the true values for the necessary safety factors, avoiding over-design or risky operation.

One of the most well-acknowledged open-access libraries used for the estimation of the thermophysical properties of various liquids and gases is CoolProp<sup>79</sup>. This library can calculate various properties, such as the density, specific heat capacity, viscosity and thermal conductivity. Density and specific heat capacity are calculated by solving the Helmholtz energy equations of state, resulting in very high accuracy. Therefore, any uncertainties related to these parameters can be neglected without significant consequences. On the other hand, properties like viscosity and thermal conductivity are calculated using various correlations from existing literature. The latter are always entailed with uncertainties that cannot be considered insignificant.

Specifically, the calculation of thermal conductivity in CoolProp is based on state-of-the-art correlations from existing literature, which rely on a theoretically based model<sup>80</sup>. For the case of normal hydrogen and parahydrogen, the proposed correlations cover a temperature range from the triple point (13.8 K) up to 1000 K and pressures up to 100 MPa. The estimated uncertainty is around 4% for temperatures >100K for the case of normal hydrogen, increasing to 7% closer to cryogenic temperatures. For parahydrogen, while uncertainty lowers at cryogenic temperatures, around 4%, it is reported only for

---

<sup>78</sup> Clarke, D. D., V. R. Vasquez, W. B. Whiting, and M. Greiner. "Sensitivity and Uncertainty Analysis of Heat-Exchanger Designs to Physical Properties Estimation." *Applied Thermal Engineering*, vol. 21, no. 10, 2001, pp. 993–1017.

<sup>79</sup> Bell, I. H., J. Wronski, S. Quoilin, and V. Lemort. "Pure and Pseudo-Pure Fluid Thermophysical Property Evaluation and the Open-Source Thermophysical Property Library CoolProp." *Industrial & Engineering Chemistry Research*, vol. 53, no. 6, 2014, pp. 2498–2508.

<sup>80</sup> Assael, M. J., M. L. Huber, R. A. Perkins, and Y. Takata. "Correlation of the Thermal Conductivity of Normal and Parahydrogen from the Triple Point to 1000 K and up to 100 MPa." *Journal of Physical and Chemical Reference Data*, vol. 40, no. 3, 2011.

pressures up to 20 MPa. For higher temperatures and higher pressures, it increases above 6%. Despite the good accuracy of the proposed correlation, there is still a need for further experimental data generation at higher pressures and temperatures <320 K, as well as liquid-phase data and data in the critical region.

The viscosity calculation of normal hydrogen is based on a correlation provided by Muzny et al.<sup>81</sup>. The correlation covers a temperature range from the triple point (13.8 K) up to 1000 K and pressures up to 200 MPa. The proposed correlation is also applicable for higher temperatures up to 2000 K; however, viscosity values are calculated under this range using extrapolation. The respective uncertainty is estimated at around 4% under cryogenic conditions (supercritical fluid phase up to 200 MPa). The region around the critical point is excluded, as uncertainties are expected to rise considerably. For higher temperatures (200 K to 400 K) and for lower pressures (< 0.1 MPa), uncertainties are expected to drop to 0.1%. For the saturated liquid phase, temperatures above 31 K, and high pressures, uncertainties are >4%. The proposed correlation was available only for normal hydrogen, while for parahydrogen no correlation was provided.

Concerning the estimation of viscosity and thermal conductivity for other mediums like nitrogen, oxygen, argon, and air, these are calculated based on correlations proposed by Lemmon and Jacobsen<sup>82</sup>. The correlations are applicable for both liquid and gaseous phases, while a simplified equation is used to enhance modelling accuracy near critical conditions. Viscosity and thermal conductivity can also be estimated for conditions below the triple point of nitrogen and argon; however, this can be achieved by using extrapolation techniques. The uncertainty of proposed correlations is estimated at around 2% in the case of nitrogen and argon for both viscosity and conductivity, while for the case of oxygen and air, the uncertainty increases to 5%. Similarly, special caution is required near the region around the critical point.

Taking everything into consideration, the main uncertainties of the thermophysical properties for various mediums are summarized in Table 9. For the purpose of Monte Carlo experiments, Gaussian distributions are assumed for all parameters. The uncertainty range reported in literature is selected for the temperature range corresponding to the expected TMS operating conditions and assumed to correspond to an interval of  $\pm 2\sigma$ .

---

<sup>81</sup> Muzny, C. D., M. L. Huber, and A. F. Kazakov. "Correlation for the Viscosity of Normal Hydrogen Obtained from Symbolic Regression." *Journal of Chemical & Engineering Data*, vol. 58, no. 4, 2013, pp. 969–979.

<sup>82</sup> Lemmon, E. W., and R. T. Jacobsen. "Viscosity and Thermal Conductivity Equations for Nitrogen, Oxygen, Argon, and Air." *International Journal of Thermophysics*, vol. 25, 2004, pp. 21–69.

**Table 9.** Summary of thermophysical properties uncertainties reported for various mediums used in Thermal Management Systems.

Parameter	Units	Type	Distribution	St. Dev. ( $\sigma$ )	Nature of Uncertainty	Ref.
Viscosity (Hydrogen)	(rel, %)	Epistemic	Gaussian	$\pm 2.0 \%$	Correlation Accuracy	[79,81]
Viscosity (Nitrogen)	(rel, %)	Epistemic	Gaussian	$\pm 1.0 \%$	Correlation Accuracy	[79,82]
Viscosity (Nitrogen)	(rel, %)	Epistemic	Gaussian	$\pm 1.0 \%$	Correlation Accuracy	[79,82]
Viscosity (Air)	(rel, %)	Epistemic	Gaussian	$\pm 2.5 \%$	Correlation Accuracy	[79,82]
Thermal Conductivity (Hydrogen)	(rel, %)	Epistemic	Gaussian	$\pm 3.5 \%$	Correlation Accuracy	[79,80]
Thermal Conductivity (Nitrogen)	(rel, %)	Epistemic	Gaussian	$\pm 1.0 \%$	Correlation Accuracy	[79,82]
Thermal Conductivity (Helium)	(rel, %)	Epistemic	Gaussian	$\pm 2.0 \%$	Correlation Accuracy	[79,82]
Thermal Conductivity (Argon)	(rel, %)	Epistemic	Gaussian	$\pm 1.0 \%$	Correlation Accuracy	[79,82]
Thermal Conductivity (Air)	(rel, %)	Epistemic	Gaussian	$\pm 2.5 \%$	Correlation Accuracy	[79,82]

Finally, all the correlations are provided for pure substances. For air mixtures, like ambient air or exhaust gases, viscosity mixing rules and blending equations can be used. One of the simplest equations is the Arrhenius equation<sup>83</sup>, shown as follows:

$$\ln(\mu_{mix}) = \sum_i^N x_i \ln(\mu_i)$$

This equation applies only for ideal mixtures and can provide a first estimation about the uncertainty of the mixture based on the respective component uncertainties by applying the chain rule as follows:

$$\frac{d\mu_{mix}}{\mu_{mix}} = \sum_i^N x_i \frac{d\mu_i}{\mu_i}$$

As is expected, due to its simplicity, this equation can be used only for the preliminary estimation of the uncertainty of the mixture. For a more accurate estimation, more complex equations should be used that also consider the non-idealities of the system<sup>83</sup>.

### The problem of heat exchanger over-design

To deal with the uncertainties in heat exchangers, designers can use the technique of “design margin” and “over-design”. For example, in some applications (i.e. shell-tube

<sup>83</sup> Zhmud, B. “Viscosity Blending Equations.” *Lube Magazine*, vol. 121, no. 93, 2014, pp. 24–27.

heat exchangers) uncertainty of the heat transfer coefficient can reach from  $\pm 10\%$  to  $\pm 15\%$ . Over-specification of the heat transfer area is typically considered during over-design. There are several issues associated however with this approach. First it can lead to control problems, regarding e.g. the control of operating temperatures. Furthermore, it can potentially lead to operability problems, concerning e.g. the actual performance of the heat exchanger, and it can lead to increased fouling. Polley and Pugh<sup>84</sup> identified that for heat exchanger systems (several heat exchangers connected in a circuit) the effect of over-design can be magnified. For example, while over-sizing the heat transfer area e.g. by  $10 \text{ m}^2$ , can increase the performance of one heat exchanger, it can lead to lower inlet temperatures for the second heat exchanger, reducing the performance of the latter. To compensate for this performance deterioration, the second heat exchanger must be over-sized by  $70 \text{ m}^2$ .

### Effect of thermal management system cryogenic pumps

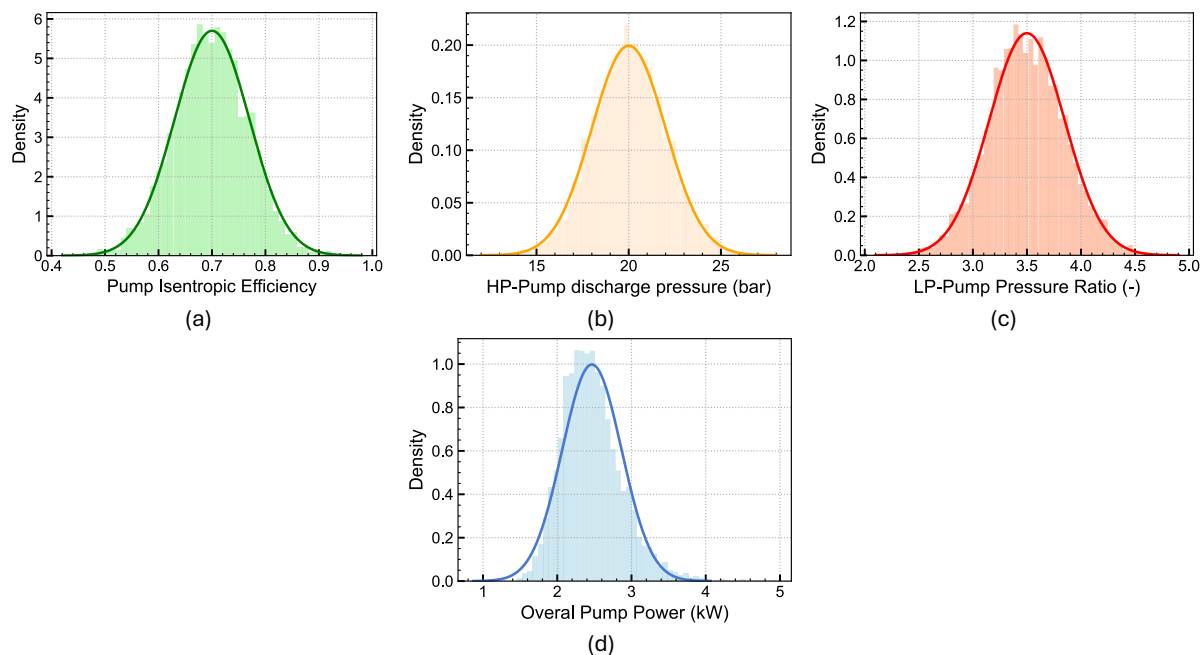


**Figure 8.** Gaussian distributions for the key operational input parameters of the cryogenic pumps (a, b, c) and the resulting effect on the overall pump power requirements (d). Despite exhibiting a non-negligible relative uncertainty, the overall power is still insignificant compared to the engine thrust power.

While the integration of the cryogenic pumps is critical for the fuel delivery, and therefore they are very important for the overall system reliability and redundancy, the effect of the cryogenic pump's main parameters on the performance of the thermal management system is rather limited. This stems from the fact that the operating mass flow rate of the pumps is orders of magnitude lower compared to the main engine mass

<sup>84</sup> Polley, G. T., and S. J. Pugh. "Dealing with Uncertainties During Heat Exchanger Design." 2001.

flow rates (<0.1%), while hydrogen as liquid, minimizes the specific work requirements. As a result, the overall pump power requirements are negligible compared to the thrust power of the aircraft engine, as well as any related uncertainty. To quantify this negligible effect, a preliminary Monte Carlo simulation analysis was conducted, considering a Gaussian distribution of a  $\pm 10\%$  standard deviation for the input parameters (pump efficiencies and pressure ratios). The resulting uncertainty of the pump overall power, illustrated in Figure 8, show that while the relative standard deviation is around  $\pm 16\%$ , even for an extreme case ( $+3\sigma$ ), the maximum pump power is still around 3.6 kW which is 0.13% compared to the maximum engine thrust power.

### Preliminary identification of thermal management system key impactful parameters

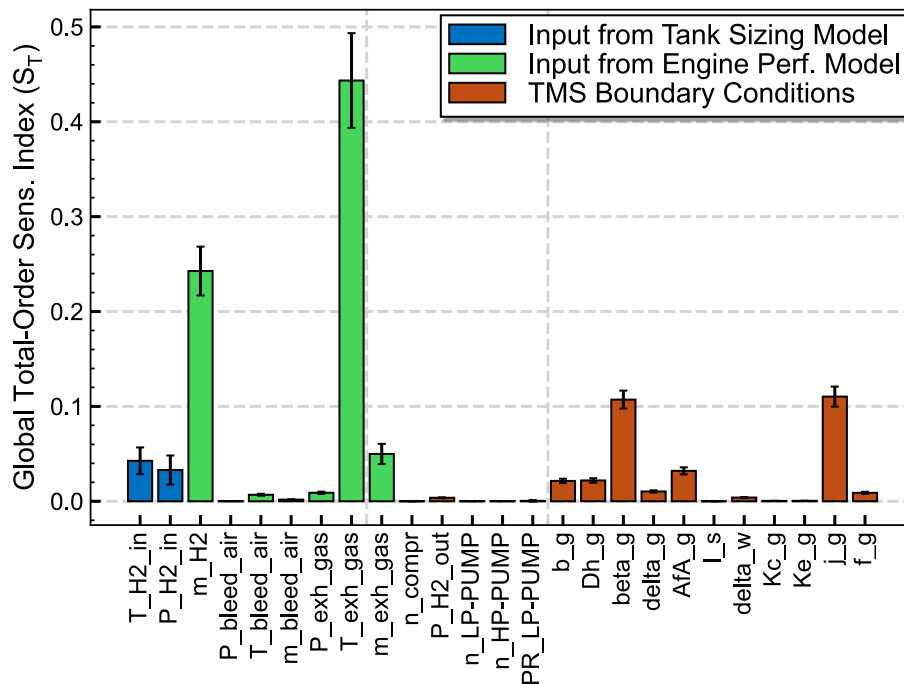


**Figure 9.** Resulting global total-order sensitivity indices of all the investigated parameters related to the TMS model.

To facilitate uncertainty analysis it is important to identify which parameters have the strongest influence on the performance of the TMS, so the characterization of their uncertainty is more critical. In this regard, a preliminary global sensitivity analysis was conducted using the Sobol’s method. Specifically, the sensitivity of 25 parameters was investigated. The selected sample to retrieve the first-order and total-order sensitivity indices was a Saltelli sample of 53,247 elements. The variability range for each parameter was selected as  $\pm 10\%$  around their nominal values in order to generate the

respective bounds. The results of the preliminary results of the implemented sensitivity analysis are summarized in Figure 9 and Table 10 which illustrates the global total-order sensitivity index for each parameter. Results show that among the various boundary conditions that are received as inputs from the engine performance model, the hydrogen mass flow rate and temperature of the exhaust gases exhibit the highest sensitivity indices. Concerning the TMS system itself, the most impactful parameters were found to be the Colburn factor and the heat exchanger compactness.

Therefore, the heat exchanger components are expected to contribute to the uncertainty propagation. The most influential parameters of the TMS are summarized in the following table. Each sensitivity index is provided with a respective confidence level, which accounts for an estimation of the uncertainty of the respective calculated indices.

**Table 10.** First-order and Total-order global sensitivity indices for the key influential parameters of the Thermal Management System.

<b>Parameter</b>	<b><math>S_1</math> (First-Order)</b>	<b><math>S_T</math> (Total-Order)</b>	<b><math>S_{T,conf}</math> (Confidence Level)</b>	<b>Integrated Model / Boundary Condition</b>
$T_{exh, gas}$	0.390	0.443	$\pm 0.050$	Engine Performance
$\dot{m}_{H_2}$	0.219	0.243	$\pm 0.026$	Engine Performance
$j_g$	0.104	0.110	$\pm 0.011$	Thermal Management System
$\beta_g$	0.095	0.107	$\pm 0.009$	Thermal Management System
$\dot{m}_{exh, gas}$	0.028	0.050	$\pm 0.011$	Engine Performance
$T_{H_2, in}$	0.006	0.043	$\pm 0.014$	Tank Sizing
$P_{H_2, in}$	-0.014	0.033	$\pm 0.015$	Tank Sizing

## 4.2. Manufacturing and measuring

As part of manufacturing the composite part of the high-pressure vessel, the uncertainty quantification pipeline is created first to identify the sources of uncertainties and investigate their propagation. Specifically, regarding the quality monitoring of the composite's part via dielectric cure sensing, Table 11 includes the detected uncertainties and their characteristics. Distribution related to measurement instruments are assumed to be normal for the time being (mainly due to noise and drift). Additionally, environmental uncertainties are pronounced through other parameters like cable's resistance and capacitance. We should bear in mind also that some uncertainties may be subjective and need further investigation. Potential changes can refer mainly to ranges and in the addition of another source of uncertainty regarding the dielectric mapping parameters, which are foreseen to have a role in the system but will be implemented in the future when we have relative information on them.

**Table 11.** Uncertainties due to composite's quality monitoring.

Parameter	Distribution	Type	Range
Resin formulation (resin/hardener ratio)	Uniform	Relative	±5% of ratio
Voltage generation	Normal (assumed)	Relative	±0.3% of value
Frequency generation	Normal (assumed)	Relative	±0.2% of value
Voltage measurement <sup>85</sup>	Normal (assumed)	Relative	±0.1% FS
Cable's resistance	Normal	Relative	±5% of value
Cable's capacitance	Normal	Relative	±10% of value
Sensor's capacitance	Uniform	Absolute	8-10 pF
ECM model accuracy (Quantity of interest $R_{resin}$ )	Normal	Relative	±2% of $R_{resin}$
Thermocouple type K	Uniform	Absolute	±0.5 K
Temperature DAQ <sup>86</sup>	Normal (assumed)	Relative	±0.3% FS

Regarding the UQ pipeline due to measurements in the HPV, Table 12 has been made. This measurement equipment is created with respect to the measurement requirements of the tank to ensure safety and the smooth operation of the tank. The uncertainty characteristics depend on the actual sensor that is going to be selected. The commercial instruments that have been selected here, and hence the corresponding uncertainty characteristics, is a suitable showcase for the usage of liquid nitrogen as a surrogate for our liquid hydrogen cryogenic storage tank. Concerning the strain sensor's distribution, it depends on the application; if the calibration happens in situ, we can treat it as normal,

<sup>85</sup> Analog voltage input module (NI 9220 datasheet): <https://www.ni.com/docs/en-US/bundle/ni-9220-specs/page/specs.html>

<sup>86</sup> Temperature DAQ (NI 9214 datasheet): <https://www.ni.com/docs/en-US/bundle/ni-9214-specs/page/specs.html>

otherwise uniform is more conservative. As a note regarding the DAQ’s large variation in its uncertainty range, it depends critically on the module type and environmental stability.

**Table 12.** Uncertainties due to measurements.

Instrument	Commercial cryogenic instrument	Measured Quantity	Units	Distribution	Type	Range
Pressure Transmitter <sup>87</sup>	GP:50 Model 7720 Cryogenic Pressure Transducer	Pressure	Pa	Normal	Relative	±0.2% FS
Thermocouples <sup>88</sup>	Omega TJ36-CAXL-116U-6	Temperature	K	Normal	Absolute	±1.0 K
Resistance Temperature Detector <sup>89</sup>	Omega PR-10 RTD Probe (PT100)	Temperature	K	Normal	Absolute	±0.35 K
Fill Level sensor <sup>90</sup>	American Magnetics Cryogenic Level Sensor (Capacitive) Vishay Micro-	Liquid Level	mm	Uniform	Relative	±1% FS
Strain sensor <sup>91</sup>	Measurements – WK-Series Cryogenic Strain Gauges	Strain	με	Normal / Uniform	Relative	±0.1 to 0.5 of reading
DAQ+modules <sup>92</sup>	NI cDAQ-9174	Voltage	V	Normal	Relative	±0.02% to 0.10% of reading

### 4.3. Operational aspects

Preliminary characterization of uncertainties concerning degradation and remaining useful life

The following discussion revolves around common uncertainties observed in traditional gas turbine engines for propulsion when evaluating engine deterioration and the associated remaining useful life (RUL). It is thought that such uncertainties will also be manifested in advanced gas turbines using LH2. Moreover, there could be some other uncertainties that are not yet known –or have not been mapped/realized–, hence not considered in our discussion.

<sup>87</sup> Pressure transmitter: [https://gp50.com/wp-content/uploads/2014/07/A5SL-053\\_7720\\_AERO\\_RwG.pdf](https://gp50.com/wp-content/uploads/2014/07/A5SL-053_7720_AERO_RwG.pdf)

<sup>88</sup> Thermocouples type T: <https://sea.omega.com/sg/techref/colorcodes.html>

<sup>89</sup> RTDs: <https://br.omega.com/omegaFiles/temperature/pdf/PR-10.pdf>

<sup>90</sup> Fill level sensor: [https://www.americanmagnetics.com/support/manuals/Model1700\\_Rev5.pdf](https://www.americanmagnetics.com/support/manuals/Model1700_Rev5.pdf)

<sup>91</sup> Strain sensor: <https://vishay-straingauge.com/pdf/strain/precision-strain-gages-sensors-1.pdf>

<sup>92</sup> DAQ: <https://www.ni.com/docs/en-US/bundle/cdaq-9174-specs/page/specs.html>

The process for tracking RUL of a traditional aeroengine is illustrated in Figure 10. The RUL for an aero engine shall be understood as the number of flight cycles (or flight hours) that are expected to be performed before the engine must be removed from on-wing operation to receive repairing.

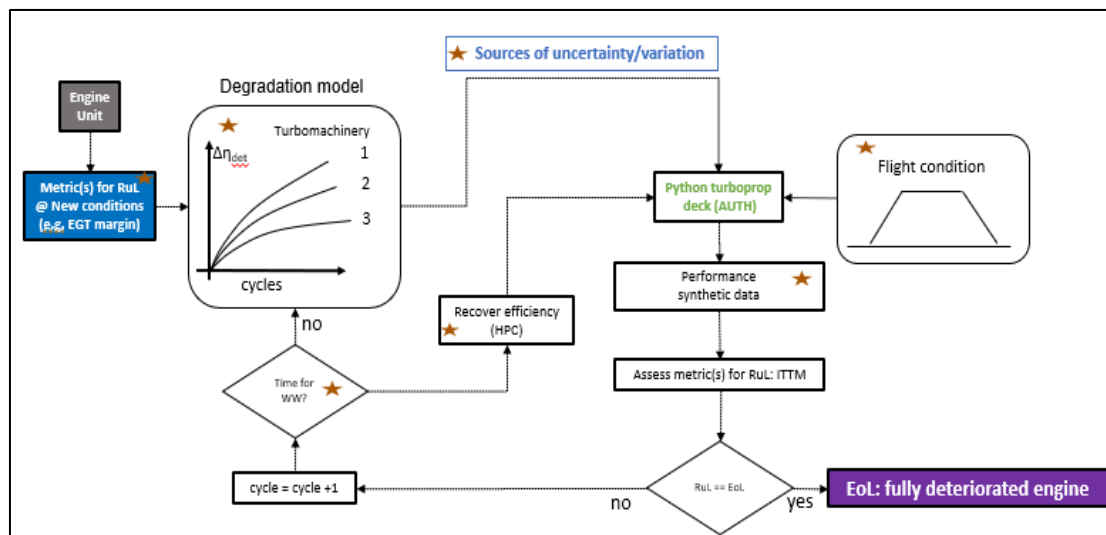


Figure 10. RUL process for aeroengines.

To track RUL, the industry (airframers, airliners, original engine manufacturers) relies on a metric, the so-called inter-turbine temperature margin (ITTM). The ITTM is the difference between a thermomechanical limit called  $ITT_{redline}$  –associated with the engine line/model in question– and the peak ITT exhibit during the take-off roll observed in each flight cycle.

The ITTM –and therefore the RUL– is maximum when the engine is in the new state condition (zero deterioration) and then degrades towards zero. When ITTM approaches zero, the RUL has been also exhausted, and the engine must be removed from in-service operation to avoid  $ITT_{redline}$  exceedances that could jeopardize the safe operation of the engine<sup>93</sup>. The reason behind the ITTM loss (or degradation) is due to the deterioration of the internal components within the turbomachinery (compressors and turbines): blades, vanes, casings, etc. Such deterioration produces efficiency losses that are translated to a deleterious overall performance of the engine, i.e., presenting higher fuel consumption and running cycle temperatures.

<sup>93</sup> AIRBUS SAS, «prevention-of-egt-overlimit-events,» Feb 2022. Available: <https://safetyfirst.airbus.com/prevention-of-egt-overlimit-events/>.

The RUL for aeroengines has shown to present a stochastic behavior, typically characterized by a normal distribution. In other words, for a given engine model/line (e.g., PW127), the group of engines (called fleet of engines) present a characteristic average and a measure of dispersion (standard deviation or variance). Consequently, it is expected to have an average RUL ( $\mu$ ) for the fleet, and the expected variation to fall between  $\mu \pm n\sigma$ . Typically,  $n$  is taken as  $n = 2.0$ , which covers about 95% of the variation in any normal distribution. For illustrative purposes Figure 11 presents the simulation of three engine units representing average, and  $\pm 2\sigma$  from a fictitious fleet of turboprop engines.

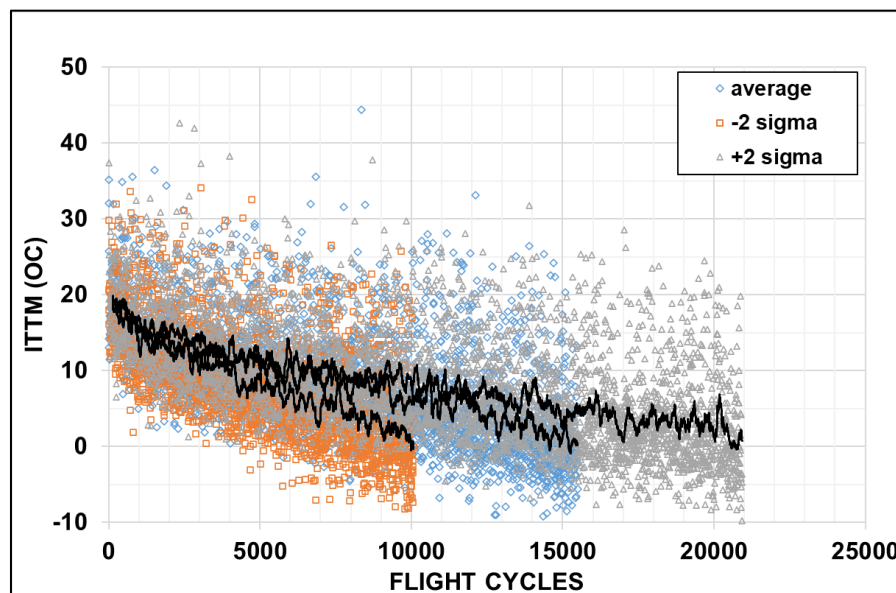


Figure 11. Illustration of three engine units presenting average, accelerated, and extended deterioration.

The RUL distribution is heavily dependent on the curve depicted by ITTM vs flight cycles. This curve is affected by several factors that play together and contribute to the overall uncertainty in the RUL. Among such factors we can list: *manufacturing/assembly quality, engine operation characteristics, maintenance actions* (e.g., cleaning). This list is not exhaustive but presents the main causes of uncertainty concerning RUL. The following paragraphs aim to describe qualitatively these factors given that reliable figures associated with them are scarce since they are proprietary information of original engine manufacturers (OEMs), and hence not disclosed to the public domain.

#### Manufacturing/assembly quality

This part refers to the different processes associated with building and assembling the different elements that constitute the turbomachinery. Engine components are manufactured by different suppliers (i.e., geographic locations), personnel (i.e., qualification levels), machines and tooling, materials (building materials, coatings),

testing (test cells), etc. Therefore, all these characteristics translate into an uncertainty that will affect the ITTM for new engine condition (zero deterioration). The only reliable information found in our literature review about the overall uncertainty of the ITTM concerning manufacturing quality was found for the General Electric (GE) CF6-6D in which the standard deviation ( $\sigma$ ) for ITTM at new production level for a sample of 82 engines is provided,  $\sigma = 8.8 \text{ }^\circ\text{C}$ <sup>94</sup>. This  $\sigma$  accounts for the impact of all the manufacturing elements previously discussed.

### Operational characteristics

The uncertainties caused by these factors are related to environmental conditions and operational practices. Aircraft engines take-off at different environmental conditions (e.g., altitudes, temperatures, and humidity levels). While ITTM is corrected to remove these effects, the corrections are not perfect and could induce some uncertainty in the final calculated ITTM. Additionally, within environmental conditions we can consider the detrimental effects caused by pollution or sandy environments. Engines have shown to present accelerated deterioration characteristics when operating in harsh or polluted environments<sup>95</sup>. Operational characteristics refer to the way pilots are recommended (or even mandated) to operate the engines within the operating manuals allowances and air traffic control recommendations. For instance, OEMs recommend airliners avoid using full-rated take offs to extend the RUL of their engine's fleet, although this might not always be possible depending on air traffic control recommendations/restrictions or airliner practices.

### Maintenance actions

While an engine remains on-wing, it is possible to perform maintenance actions that do not require actual mechanical repairing. This procedure consists in washing the fan blades and the core of the engine with high-pressure water jets along with non-abrasive chemical agents. Such cleaning process allow to remove the particles that attach to the aerodynamic surfaces in the engine and hence recover efficiency. Depending on how often the engines are washed and the quality of cleaning process, the recovery can be between 7-10  $^\circ\text{C}$ <sup>96</sup>. The procedure of cleaning the engine is highly recommended for engines operating in polluted and/or sandy environments.

---

<sup>94</sup> Wulf, Ray (General-Electric), «CF6-6D Engine Performance Deterioration,» NASA, 1980.

<sup>95</sup> L. W. J. F. Tobias Wensky, «Environmental Influences on Engine Performance Degradation,» ASME Turbo Expo, 2010.

<sup>96</sup> Hutter, Ivan (GE Aviation), «ICAO,» Septembre 2026.

Available: <https://www.icao.int/Meetings/EnvironmentalWorkshops/Documents/ICAO-TransportCanada-2006/Hutter.pdf>

## Margins related to deterioration

Every aircraft engine is also expected to degrade its performance over time for various reasons (i.e., compressor fouling due to foreign object impacts, etc.). This can reduce the component efficiencies, resulting in a deterioration of the overall performance. For each engine operating for 10000 h, a degradation in performance is expected, expressed as +3% to +6% in the SFC and -5% to -15% in the engine power. To ensure the engine will deliver the required power even under degradation, a slightly higher design power should be considered to account for any potential power loss. This, according to the PW127 engine maintenance manual can be accounted for with a margin of 30K in the TET design constraint.

## Uncertainty quantification of engine degradation

Ellis et al.<sup>97</sup>, also created a novel approach that couples particle deposition and aero-engine performance models to predict operational capability. In more detail, Monte Carlo simulations were used to statistically quantify the performance degradation in a Rolls-Royce RB211-524C engine resulting from ingestion of volcanic ash and dust. The approach coupled a 1D (Numerical Propulsion System Simulation) NPSS performance model with a reduced-order particle deposition model, allowing rapid simulation across thousands of runs. The methodology included a gas turbine performance model using NPSS and validated on 20 mission operating points at cruise level. The particle deposition model was created by a reduced-order deposition algorithm that computed accumulation factor using interaction probability and retention probability that affect nozzle guide vane throat area. Finally, using the Monte Carlo framework, around 4,000 MC runs were performed, sampling uncertain input variables like cloud concentration, exposure duration, and particle properties like mean sphericities. Then, these were propagated through the coupled model to simulate the NGV throat area reductions and resulting engine health metrics

To conclude, providing realistic predictions of the potential uncertainties concerning the deterioration and RUL of disruptive propulsion systems—such as gas turbine engine running with LH2 considered in DEMOQUAS—; first, we need to look at the learnings gathered from traditional propulsion engines. As briefly presented in this section, the uncertainties concerning engine degradation and RUL encompass *manufacturing/assembly quality, operational characteristics, and maintenance*. Although, it is highly likely additional sources of uncertainties will be associated with the specific challenges of using LH2.

---

<sup>97</sup> Ellis M., Bojdo N., Filippone A., and Clarkson R. "Monte Carlo Predictions of Aero-Engine Performance Degradation Due to Particle Ingestion." *Aerospace*, vol. 8, no. 6, 2021, p. 146.

## Annex

### Calculation of compact offset strip plate-fin heat exchanger dimensions

The calculation of the main geometrical parameters of a compact heat exchanger featuring an offset strip plate-fin geometry is based on a methodology proposed by Shah and Sekulic<sup>76</sup>. A typical geometry schematic is shown in Figure 6. These geometries typically feature standardized dimensions proposed by Kays and London<sup>77</sup>. The standardized input dimensions that are provided for each selected geometry are:

- Plate spacing for each side ( $b_1, b_2$ )
- Fin offset length ( $l_s$ )
- Fin and plate thickness ( $\delta, \delta_w$ )
- Fin pitch ( $p_f$ ), which is the number of fins for each length unit

Furthermore, to calculate the key geometrical parameters of the heat exchanger, the core component dimensions are necessary, specifically:

- Overall length and the cold-side ( $L_1$ ) and hot-side ( $L_2$ ), as well as the height ( $L_3$ ).
- Total number of cold passages ( $N_p$ ). For the hot side, it is assumed that includes  $N_p + 1$  passages.

Based on the given inputs first the following parameters are estimated:

$$\text{– Number of fins per passage: } n'_f = L_2/p_f \quad (\text{A. 1})$$

$$\text{– Total number of fins: } n_f = n'_f \cdot N_p \quad (\text{A. 2})$$

$$\text{– Number of fin offsets: } n_{off} = L_f/l_s \text{ where } L_f \approx L_1 \quad (\text{A. 3})$$

The total primary area can be then calculated as:

$$A_p = 2L_1L_2N_p - 2\delta L_f n_f + 2b_1L_1N_p + 2(b_2 + 2\delta_w)(N_p + 1)L_2 \quad (\text{A. 4})$$

The total secondary (fin) area  $A_f$  is calculated correspondingly:

$$A_f = 2(b_1 - \delta)L_f n_f + 2(b_1 - \delta)\delta n_{off} n_f + (p_f - \delta)\delta(n_{off} - 1)n_f + 2p_f \delta n_f \quad (\text{A. 5})$$

Based on the latter the overall heat transfer area ( $A$ ) can be calculated which lead to the estimate of the fin area-to-total area ratio ( $A_f/A$ ).

$$A = A_p + A_f \quad (\text{A. 6})$$

Then, the total heat transfer area/volume between plates ( $\beta$ ) is calculated as follows:

$$\beta = \frac{A}{L_1L_2b_1N_p} \quad (\text{A. 7})$$

The minimum free-flow area ( $A_o$ ) can be also calculated:

$$A_o = b_1L_2N_p - [(b_1 - \delta) + p_f]\delta n_f \quad (\text{A. 8})$$

Which ultimately leads to the calculation of the hydraulic diameter:

$$D_h = \frac{4A_{o,1}L_1}{A} \quad (\text{A. 9})$$